Rec8 cohesin-mediated loop-axis chromatin architecture is required for meiotic recombination

Takeshi Sakuno[1*#], Sanki Tashiro[2#], Hideki Tanizawa[2], Osamu Iwasaki[2], Da-Qiao Ding[3], Tokuko Haraguchi[1], Ken-ichi Noma[2, 4*] and Yasushi Hiraoka[1*]

[1] *Graduate School of Frontier Biosciences, Osaka University, Suita 565-0871, Japan;*

[2] *Institute of Molecular Biology, University of Oregon, Eugene, OR 97403, USA;*

[3] *Advanced ICT Research Institute Kobe, National Institute of Information and Communications Technology, Kobe 651-2492, Japan;*

[4] *Institute for Genetic Medicine, Hokkaido University, Sapporo 060-0815, Japan*

# These authors contribute equally to this work.

*Corresponding authors: Takeshi Sakuno (sakuno@fbs.osaka-u.ac.jp) and Yasushi Hiraoka (hiraoka@fbs.osaka-u.ac.jp), Graduate School of Frontier Biosciences, Osaka University, Suita 565-0871, Japan; Ken-ichi Noma (noma@uoregon.edu), Institute of Molecular Biology, University of Oregon, Eugene, OR 97403, USA.

Summary

During meiotic prophase, cohesin-dependent axial structures are formed in the synaptonemal complex (SC). However, the functional correlation between these structures and cohesion remains elusive. Here, we examined the formation of the cohesin-dependent axial structure in fission yeast, which forms atypical SCs composed of linear elements (LinEs) resembling the lateral elements of SC but lacking the central elements. The results demonstrated that Rec8 cohesin is crucial for the formation of the loop-axis structure within the atypical SC. Furthermore, the Rec8-mediated loop-axis structure is formed in the absence of LinEs and provides a structural platform for aligning homologous chromosomes. We also identified a *rec8* mutant that lost the ability to assemble the loop-axis structure without losing cohesion. Remarkably, this mutant showed defects in the LinE assembly, resulting in a significant reduction in meiotic recombination. Collectively, our results demonstrate an essential role for the Rec8-dependent loop-axis structure in LinE assembly, facilitating meiotic recombination.

Keywords

meiosis, cohesin, Rec8, chromosome, axis-loop structure, recombination, fission yeast, linear element, miscarriage, developmental disorders

Introduction

Meiosis is a unique type of cell cycle for sexual reproduction, which halves the chromosome number by two successive nuclear divisions after a single round of DNA replication to produce haploid gametes. In the first meiotic division (meiosis I), homologous chromosomes (homologs) are segregated to opposite poles. This type of division is called reductional segregation and is essentially different from mitosis or meiosis II, in which sister chromatids are segregated to opposite poles (Petronczki et al., 2003). Crossovers formed by reciprocal recombination constitute a physical link between homologs, ensuring reductional segregation (Hunter, 2015; Zickler and Kleckner, 1999). Failure to establish such interhomolog links leads to the mis-segregation of chromosomes during meiosis I, resulting in aneuploidy of gametes. This is a major cause of human miscarriage or developmental disorders caused by chromosome trisomy, such as Down syndrome (Nagaoka et al., 2012; Webster and Schuh, 2017).

During meiotic prophase, homologs become closely associated or aligned through an elaborate proteinaceous structure called the synaptonemal complex (SC), followed by crossover recombination. The SC consists of two lateral elements, each along the axis joining a pair of sister chromatids, with one central element connecting the lateral elements (Grey and de Massy, 2021; Kleckner, 2006). The process of chromatin loop formation is thought to be essentially mediated by meiotic cohesin (Klein et al., 1999; Petronczki *et al.*, 2003). The cohesin complex is responsible for sister chromatid cohesion. The complex consists of two structural maintenance of chromosome (SMC) proteins, a kleisin subunit, and a stromal antigen (SA) subunit. Replacement of kleisin commonly occurs in most organisms, in which the somatic kleisin Rad21/Scc1 is replaced by Rec8

63 during meiosis (Ishiguro, 2019; Mehta et al., 2013; Nasmyth, 2001). Rec8 cohesin is
64 responsible for sister chromatid cohesion and provides a physical link between homologs
65 as a result of crossover (Moore and Orr-Weaver, 1998; Petronczki *et al.*, 2003).
66 Additionally, Rec8 cohesin is required for the assembly of lateral elements in diverse
67 eukaryotes (Cai et al., 2003; Fujiwara et al., 2020; Fukuda et al., 2014; Golubovskaya et
68 al., 2006; Hopkins et al., 2014; Ishiguro et al., 2014; Klein *et al.*, 1999; Llano et al., 2014;
69 Pasierbek et al., 2001; Winters et al., 2014; Xu et al., 2005). A recent study using high-
70 throughput chromosome conformation capture (Hi-C) (Lieberman-Aiden et al., 2009) in
71 the budding yeast *Saccharomyces cerevisiae* clearly revealed that Rec8 cohesin is
72 essential to construct meiosis-specific chromatin loop structures (Schalbetter et al., 2019).
73 As studied in somatic cells, cohesins can form higher-order structures by pulling together
74 distant regions of the chromosome, for which a loop extrusion model has been proposed
75 (Davidson and Peters, 2021; Fudenberg et al., 2016; Kim et al., 2019; Mizuguchi et al.,
76 2014; Rao et al., 2017; Sanborn et al., 2015). Pds5 and Wpl1/Wapl are cohesin-
77 associating factors conserved in yeasts and vertebrates. These are considered to dissociate
78 cohesin from chromatin (Challa et al., 2019; Peters and Nishiyama, 2012), thus affecting
79 higher-order chromosome structures (Challa et al., 2016; Crawley et al., 2016; Ding et al.,
80 2016a; Ding et al., 2006; Haarhuis et al., 2017; Hong et al., 2019; Silva et al., 2020;
81 Tedeschi et al., 2013; Viera et al., 2020).
82
83 The fission yeast *Schizosaccharomyces pombe* forms an atypical SC composed of a
84 structure called the linear element (LinE). The LinE resembles the lateral element of the
85 SC, but lacks central element components, such as *S. cerevisiae* Zip1 (Bähler et al., 1993;
86 Davis et al., 2008; Estreicher et al., 2012; Loidl, 2006; Lorenz et al., 2004; Olson et al.,

87 1978). Full alignment of homologs in *S. pombe* is finally achieved by chiasmata formation
88 following crossover recombination (Loidl, 2006). The recognition and alignment of
89 homologs in *S. pombe* relies on oscillatory movement of the nucleus (horsetail
90 movement) in a bouquet orientation with all telomeres clustered to the spindle pole body
91 (SPB) (Chikashige et al., 1994; Ding et al., 1998; Ding et al., 2019; Hiraoka, 2020; Loidl,
92 2006; Yamamoto and Hiraoka, 2001). More recently, a mechanism was proposed in which
93 noncoding RNA on chromatin contributes to the initial recognition of correct homolog
94 pairs (Chikashige *et al.*, 1994; Ding *et al.*, 1998; Ding *et al.*, 2019; Hiraoka, 2020; Loidl,
95 2006; Yamamoto and Hiraoka, 2001).
96
97 Importantly, it has been shown that the phosphorylation of Rec11, a homolog of the
98 meiosis-specific SA3 subunit of Rec8 cohesin in *S. pombe*, by casein kinase 1δ/ε (CK1),
99 is required for the assembly of LinEs (Phadnis et al., 2015; Sakuno and Watanabe, 2015).
100 The Rec8 cohesin complex containing phosphorylated Rec11 specifically interacts with
101 Rec10, a homolog of the lateral element factor Red1/SYCP2. Previous studies in mouse
102 spermatocytes have shown that depletion of the SYCP2 or SYCP3 structural components
103 of axial elements causes defects in axial element formation despite normal cohesin-axis
104 (Fujiwara *et al.*, 2020; Fukuda et al., 2010; Pelttari et al., 2001). Accordingly, the
105 structural property of chromatin to trail the horsetail movement is maintained in LinE-
106 defective mutants of *S. pombe* (Ding *et al.*, 2006; Sakuno and Watanabe, 2015). Based on
107 these observations, it should be emphasized here that the Rec8-dependent chromosomal
108 structure is strictly independent of lateral elements (or LinEs in *S. pombe*). However, the
109 significance of the Rec8-dependent axis-loop structure in meiotic recombination remains
110 unclear.

111

112 In this study, we performed Hi-C analysis to describe the meiotic chromosome structures
113 of *S. pombe* in detail. We then sought to clarify the functional significance of the Rec8-
114 dependent loop-axis structure by identifying *rec8* mutants that specifically show defects
115 in axis formation, but not in cohesion. The collective data demonstrate that the Rec8-
116 dependent loop-axis structure itself provides the scaffold to assemble the LinE axis,
117 facilitating the execution of reciprocal recombination.

118

119 **Results**

120 **Induction of highly synchronized meiosis under physiological conditions**

121 To achieve Hi-C analysis of chromosomal configurations during meiotic prophase, we
122 first developed an experimental system to prepare *S. pombe* cell populations undergoing
123 highly synchronized meiotic progression under physiological conditions. For this purpose,
124 we employed an *h-/h- pat1-as2/pat1-as2* diploid strain harboring one copy of the *mat*-Pc
125 gene cassette (Cipak et al., 2012; Funaya et al., 2012; Yamamoto and Hiraoka, 2003).
126 Meiosis can be induced using this ATP analog-sensitive allele of the Pat1 kinase (*pat1-*
127 *as2*) upon inactivation of the Pat1 kinase by addition of the ATP analog, instead of the
128 temperature-sensitive allele (*pat1-114*), in which raising temperature has detrimental
129 effects on meiosis (Bähler et al., 1991; Cipak *et al.*, 2012). In addition, MDR-sup alleles
130 (Aoi et al., 2014; Kawashima et al., 2012), which allow efficient cellular uptake of ATP
131 analogs, were also exploited. As shown in Figure S1A, the meiotic progression of wild
132 type diploid cells harboring Rec8-green fluorescent protein (GFP) was highly
133 synchronous (~70%), as indicated by the timing of nuclear division in meiosis I. Pre-
134 meiotic DNA replication was almost completed approximately 1.5 hours after the

135 induction of meiosis by the addition of an ATP analog after G1-arrest via nitrogen
136 starvation (Figure S1A, left panel).
137
138 **Hi-C analysis recapitulates meiotic bouquet chromosomes in *S. pombe***
139 For Hi-C analysis, cells were collected at 0 h (G1) and 2.5 h (meiotic prophase) after
140 meiosis induction, along with cells in vegetative growth (VG; mainly in mitotic G2 phase).
141 Notably, even at 0 h, a significant amount of Rec8-GFP protein was expressed and loaded
142 onto chromatin. The amount of Rec8 peaked at approximately 2.5–3 h after meiotic
143 induction (Figures S1B and S1C). Hi-C contacts of all three chromosomes in VG cells
144 detected obvious centromere clustering (indicated by green arrowheads in Figures 1B and
145 1C), suggesting the organization of the Rabl orientation (Figure 1A, left). In contrast, as
146 cells progressed from G1 to meiotic prophase, centromere clustering became vague, while
147 telomere clustering became evident (Figures 1B and 1C; blue arrowhead). Remarkably,
148 as cells entered the meiotic prophase, X-shaped inter- and intra-chromosomal contacts
149 appeared (Figures 1B and 1C). These X-shaped contact patterns represent chromosomal
150 arms bundled at the telomere (Figure 1A; right), as previously demonstrated in *S. pombe*
151 meiotic prophase (Chikashige et al., 1997; Ding *et al.*, 1998). The degree of alignment
152 along the intra-chromosomal arms from the telomere was quantified by the "alignment
153 index" (Figure S1D). The alignment index of chromosome 1 increased from 1.6 (onset of
154 meiosis at 0 h) to 2.5 (meiotic prophase at 2.5 h) compared with 0.55 in VG (Figure 1D).
155 A similar structure was observed during meiotic prophase in mouse spermatocytes by Hi-
156 C analysis, although it was not as evident as in *S. pombe* (Patel et al., 2019).
157
158 **Rec8 cohesin produces a chromosome shape suitable for alignment**

159 Next, we examined three factors that play a central role in meiotic recombination. Rec10
160 is a major component of LinE. Rec12 is a Spo11 homolog that induces DNA double-
161 strand breaks (Keeney, 2001; Sharif et al., 2002). Rec8 is a meiotic cohesin. To
162 investigate their contributions to meiotic chromosome structures, we confirmed
163 synchronous progression of meiosis in these mutants and performed Hi-C analyses
164 (Figure S2). *rec10*Δ and *rec12*Δ cells showed slight defects in formation of the X-shaped
165 contacts (Figures 2A and 2B), with an alignment index of 2.8 (*rec10*Δ), 2.5 (*rec12*Δ), and
166 2.5 (*wild type*, *wt*). In contrast, *rec8*Δ cells showed prominent defects with almost no X-
167 shaped contacts (Figures 2A and 2B; alignment index 1.5). These findings suggest that
168 Rec8 regulates the alignment of homologs in a manner distinct from LinE formation to
169 modulate recombination. The bulk of the chromosomes do not follow the horsetail
170 movement at meiotic prophase in *rec8*Δ, while only telomere regions follow the leading
171 edge of the moving nucleus (Ding et al., 2016b; Ding *et al.*, 2006). These observations
172 imply that the traction force generated by the horsetail movement is not transmitted to the
173 chromosomes in *rec8*Δ, leading to the loss of alignment along the chromosomes.
174 Therefore, Rec8 cohesin likely provides the chromosome with appropriate structural
175 properties to counteract the pulling force, independent of LinEs (Figure 3F).
176
177 **Rec8 cohesin is crucial to form meiosis-specific chromatin loops**
178 Magnification of Hi-C data (2 kbp binning) in chromosome arm regions revealed that
179 punctate Hi-C interactions occurred at the onset of meiosis (0 h) and became more
180 prominent as meiosis progressed (2.5 h) in the wild type (arrows in Figures 3A and S3A).
181 The positions at the bases of these interactions markedly coincided with the previously
182 identified Rec8 accumulation sites (Ito et al., 2014) (Figures 3B and S3B). Consistently,

183 as meiosis progressed in the wild type, *P(s)* (the contact frequency versus distance)
184 indicated a "shoulder" at approximately 50 kbp, representing an increase in interactions
185 within a region shorter than that length (Figure 3C). Crucially, punctate Hi-C interactions
186 observed in the wild type were mostly lost in *rec8*Δ, but were retained in *rec10*Δ or *rec12*Δ
187 (Figures 3A and S3A). In addition, the shoulder in *P(s)* was lost in the *rec8*Δ mutant, but
188 not in *rec10*Δ or *rec12*Δ (Figure 3D). These data suggest the linear compaction of
189 chromosomes and the emergence of a Rec8-dependent *cis*-loop structure upon entry into
190 meiosis in the wild type. In the Hi-C data of 5 kbp binning, topologically associating
191 domain (TAD)-like signals were observed in wild type VG cells (dotted lines in Figure
192 3E), representing relatively long-range interactions manifest in mitotic chromosomes
193 (Kim et al., 2016; Mizuguchi *et al.*, 2014; Patel *et al.*, 2019; Tanizawa et al., 2017).
194 Interestingly, as Rec8-dependent loop structures appeared during meiosis, these TAD-like
195 signals disappeared. Thus, *S. pombe* chromosomes undergo a structural transition through
196 Rec8-dependent formation of chromatin loop-axis structures upon entry into meiosis
197 (Figure 3F).
198
199 **Wpl1 in *S. pombe* regulates the length of chromatin loops in meiotic prophase**
200 In Rad21/Scc1 cohesin-dependent chromatin organization with TADs in somatic cells,
201 Wapl depletion lengthens the chromatin loops and thickens the chromatin axis (Haarhuis
202 *et al.*, 2017; Tedeschi *et al.*, 2013). However, it is unknown whether Rec8-dependent
203 chromatin loops are affected by Wapl during meiosis. As shown in Figure 4A, the meiotic
204 chromosome axial structures observed by Rec8-GFP were more prominent in *wpl1*Δ than
205 in the wild type, suggesting that the axial structure becomes thicker in *S. pombe* meiosis.
206 To examine the chromosome structure in *wpl1*Δ, we performed Hi-C analysis as in the

207 wild type (Figure S4A). In the Hi-C contact maps in *wpl1*Δ (Figure 4B, upper), the
208 background was lower than that in the wild type (compare with Figure 1B and the lower
209 panel of Figure 4B). These findings suggest that the inter- and intra-chromosomal long-
210 range interactions, including X-shaped contacts, were reduced in *wpl1*Δ, which has a
211 thicker chromatin axis, compared to the wild type (see Figure S4E).
212
213 In the amplified view of Hi-C data (2 kbp binning) in *wpl1*Δ, the number of grid-like
214 punctate signals increased and the size of the diagonals of each grid increased upon entry
215 into meiosis (Figures 4C and S4B). These findings imply that the nearby chromatin loops
216 are in contact with each other at their bases with longer loops and thicker axes, leading to
217 the linear compaction of chromosomes (Figure S4C). Consistently, compared to that of
218 the wild type, a rightward shift of the shoulder in the *P(s)* (blue dotted line for *wt* and
219 green dotted line for *wpl1*Δ in Figure 4D) and an increase in longer loop formation (Figure
220 4E) were observed in *wpl1*Δ. Note that, because axial signals of Rec8-GFP were still
221 thicker in the absence of LinEs (*wpl1*Δ *rec10*Δ double mutant, Figure S4D), Rec8 loop-
222 axis structures formed independently of LinEs, even under the condition of *wpl1*Δ. These
223 results strongly indicate that Wpl1/Wapl can antagonize the construction of chromosomal
224 axes restricting chromatin loop extension, even when mediated by meiotic Rec8 cohesin
225 in *S. pombe* (Figure S4C).
226
227 **Identification of *rec8* mutants showing defects in axis formation**
228 The foregoing results demonstrate that Rec8 cohesin is crucial for the formation of the
229 meiosis-specific axis-loop structure in *S. pombe* meiosis. Importantly, ectopic expression
230 of Rad21 cohesin in meiosis partly compensates for the cohesion defect in the absence of

231 Rec8 (Kitajima et al., 2003; Yokobayashi et al., 2003). However, Rad21 signals were
232 obscure along the chromatin axis (Figure S5A). Thus, besides cohesion, Rec8 may have
233 an additional function that is more robust than Rad21 in chromatin axis formation.
234 Therefore, it is possible to identify the mutant of *rec8* that specifically shows defects in
235 axis formation without affecting its cohesion function. To explore this, we examined the
236 *S. pombe* strain in which Rec8 and Rec11 were ectopically expressed as the sole source
237 of cohesin during mitosis, replacing Rad21 and Psc3 (Figure 5A). Using this strain as a
238 screening host, randomly mutagenized *rec8* cDNAs fused with GFP-coding DNA were
239 transformed into the host strain. Since Rec8 is the only available kleisin protein in this
240 strain, transformants will show a lethal or slow-growth phenotype if there is a *rec8*
241 mutation that causes loss of cohesion. Moreover, using the h^{90} mating-type and *mei4*Δ
242 background, each transformant arrests at the meiotic prophase on agar plates of
243 sporulation medium (Horie et al., 1998). We also introduced *wpl1*Δ in the host strain to
244 produce the prominent axis of Rec8-GFP (Figure 4A) so that defects in axis formation
245 can be easily evaluated by microscopy observation (Figure 5A). Deletion of $mei4^{+}$
246 represses the expression of recombination-related factors such as Rec12, resulting in
247 almost no recombination (Miyoshi et al., 2012; Murakami-Tonami et al., 2007; Young et
248 al., 2004). However, in the present study this did not seem to affect the Rec8 axis
249 formation, at least in the *wpl1*Δ background (Figure S5B).
250
251 We searched approximately 3000 viable transformants of the *rec8* mutant library for
252 mutants that showed axis formation defects with normal cohesion function in
253 fluorescence microscopy. We identified a mutant that displayed normal growth (Figure
254 S5C) but lost the Rec8 axis structure (Figure 5B). In this mutant, phenylalanine at amino

255 acid residue 204 of Rec8 was substituted with serine (*rec8-F204S*). Strikingly, sister
256 chromatid cohesion was preserved in the *rec8-F204S* mutant, as assessed at the *cut3* gene
257 locus (Figure 5C) and other chromosomal loci (Figure S5D). In the cohesion assays, we
258 used *rec8-S552P* or *rec8*Δ, which showed the cohesion defect, as a control strain (Figures
259 5C and S5D). The *rec8-S552P* mutant showed normal growth during mitosis (Figure
260 S5C), but displayed defects in axis formation and cohesion during meiosis, probably due
261 to low protein expression or low stability of the Psm1 subunit in the cohesin complex
262 (Figure S5E and S5F). Although cohesion defects are expected to occur during mitosis of
263 the P_{adh1}-derived *rec8-S552P* strain (Figure S5C), growth would be ensured by their
264 overexpression. Since the backup of Rad21 is likely to function only in *rec8*Δ cells, the
265 *rec8-S552P* mutant was more deficient in cohesion than *rec8*Δ (Figures 5C and S5D).
266 The cohesin complex seemed to be formed normally in the *rec8-F204S* mutant with
267 comparable expression of Rec11 (Figures S5G and S5H). The F204 of Rec8 seemed to
268 be conserved among Rec8 species in other organisms (Figure 5D), implying the
269 significance of this residue in regulating Rec8 functions. Furthermore, the analysis of
270 mutants in which F204 was replaced by amino acids other than serine indicated that the
271 hydrophobicity of this position of Rec8 may be important for its axis-forming function,
272 independent of its cohesion function (Figure S5I).
273
274 Thereafter, to delineate the details of axis formation defects caused by *rec8-F204S*, we
275 observed chromosome morphology during horsetail movement in meiotic prophase. In
276 the *rec8-F204S* mutant, only the nuclear leading edge followed the horsetail movement
277 with the bulk of chromosomes remaining, similar to *rec8*Δ, in which axial assembly and
278 chromosome compaction were lost (Figure 5E, Supplemental Movies 1, and 2). To

279 determine the degree of chromosome compaction more directly, we measured the distance
280 between the telomere and the *ade8* gene locus during meiotic prophase using a GFP-
281 tagged telomere protein (Taz1) and a *lacO*/lacI-GFP tag at the *ade8* gene locus (Figure
282 5F). As in *rec8*Δ, the telomere-*ade8* distance was longer in the *rec8-F204S* mutant than
283 in the wild type, suggesting that the chromatin of the *rec8-F204S* mutant is flexible and
284 is abnormally stretched by the traction of horsetail movement.
285
286 ***rec8-F204S* mutant is defective in chromatin loop formation**
287 Next, we performed Hi-C analysis in the *rec8-F204S* mutant as in the *rec8-wt* (Figure
288 S6A). In the Hi-C contacts of three chromosomes at meiotic prophase (2.5 h), formation
289 of X-shaped contacts representing the bouquet orientation were apparently compromised
290 in the *rec8-F204S* mutant, similar to *rec8*Δ (Figure 6A). The alignment index of
291 chromosome 1 at meiotic prophase (2.5 h) decreased in *rec8-F204S* (1.6) compared with
292 the wild type (*rec8-wt*, 2.6) (Figure 6B). The findings were consistent with the fact that
293 chromatin is too flexible to resist the traction of horsetail movement in the *rec8-F204*S
294 mutant (Figures 5E and 5F). Moreover, in the amplified 2 kbp binning view of Hi-C data,
295 a clear decrease in the punctate Hi-C interactions was observed in *rec8-F204S*, although
296 it was not as prominent as in *rec8*Δ (Figure 6C). In addition, the shoulder in *P(s)* became
297 flattened in *rec8-F204S* compared with *rec8-wt*, both at 0 h and 2.5 h after meiosis
298 induction (Figure 6D). Consistently, chromatin loops with a length of approximately 20
299 kbp that formed in a Rec8-dependent manner were diminished at meiotic prophase in
300 *rec8-F204S* (Figure 6E). These findings suggest that in the *rec8-F204S* mutant, as in
301 *rec8*Δ, the Rec8-dependent meiosis-specific short chromatin loop structures are lost,
302 resulting in a concomitant loss of the structural property of the chromosome required for

303 proper alignment. Next, we performed a chromatin immunoprecipitation (ChIP) assay to
304 determine the localization pattern of Rec8 on chromatin. The accumulation of Rec8-
305 F204S protein apparently decreased compared with wild type Rec8 at the loci of known
306 cohesin-enriched regions. In contrast, the localization in other chromosome arm regions
307 seemed to be normal (Figure S6B). Rec8-enriched regions mostly coincided with each
308 base of the chromatin loops (Figures 2B and S2B). In the case of *rec8-F204S*, the amount
309 of Rec8 of in the non-enriched region appeared normal. Thus, the reduced Rec8
310 probability at known enriched regions possibly reflects the noticeable loss of chromatin
311 loop formation (Figure S6C).
312

313 **Rec8-dependent axis-loop structure is required for LinE formation and**
314 **recombination**

315 To delineate the significance of the Rec8-dependent axis-loop structure in terms of
316 meiotic recombination, we examined the formation of LinEs during meiotic prophase. In
317 wild type cells, the LinE component Rec10, marked by mCherry, localized within the
318 entire nucleus, similar to Rec8 (Figures 7A and S7A; *CK1*$^{+}$, *rec8*$^{+}$, *rec11-wt*). In *rec8-*
319 *F204S* cells, however, Rec10-mCherry formed aberrant dotty or filamentous aggregates
320 within the nucleus (Figures 7A and S7A), as with *rec8*Δ or *rec11-5A*, in which LinE was
321 completely lost (Sakuno and Watanabe, 2015). Interestingly, Rec11 phosphorylation by
322 CK1, which is required for the assembly of LinEs (Sakuno and Watanabe, 2015), occurred
323 normally in the *rec8-F204S* mutant, similar to the wild type (Figure 7B). We also
324 expressed mimetic mutations of CK1-mediated phosphorylation of Rec11 (*rec11-5D*),
325 which can suppress the defects caused by the loss of Rec11 phosphorylation via CK1
326 (Sakuno and Watanabe, 2015). Strikingly, the expression of Rec11-5D protein did not

327 suppress defects in LinE formation or meiotic recombination in *rec8-F204S* (Figures S7A
328 and S7B). These results strongly suggest that axis-loop formation along sister chromatids
329 via Rec8 cohesin is still essential for LinE assembly, even in the presence of active CK1-
330 dependent regulation. Consistent with the LinE formation defect, *rec8-F204S* cells
331 showed a decreased frequency of crossover recombination at several loci (Figure 7C).
332 Intragenic recombination between the genomic *ade6-M26* allele and plasmid harboring
333 the *ade6-469* allele was also significantly reduced in *rec8-F204S*, similar to *rec8*Δ (Figure
334 S7C). Collectively, these results demonstrate the essential role of the Rec8-dependent
335 loop-axis structure, which may function as a scaffold for LinE assembly, thus facilitating
336 meiotic recombination.
337

338 **Discussion**

339 We demonstrate the Rec8-dependent formation of axis-loop structures during meiosis in
340 *S. pombe,* an asynaptic organism. The Rec8 cohesin functions as a scaffold for the
341 formation of the LinE axis, thereby ensuring meiotic recombination during meiosis.
342

343 **Pairing of homologous chromosomes in *S. pombe* meiosis**

344 Our Hi-C analysis revealed the emergence of an intriguing X-shaped contact map
345 representing tight contacts between chromosome arm regions near the telomere in *S.*
346 *pombe* meiotic prophase. This is consistent with the previous microscopy observation of
347 telomere clusters at the SPB (the bouquet orientation of chromosomes) during meiotic
348 prophase (Chikashige *et al.*, 1994; Ding *et al.*, 1998). The Hi-C data indicate that contacts
349 also occur between non-homologous arms, not only between homologous arms. It should
350 be noted that chromosomes recognize their homologous partners to pair within the bundle

351 of all chromosomes. Therefore, there must be mechanisms to eliminate non-homologous
352 pairing, while simultaneously promoting homologous pairing. Such selective forces
353 between chromosomes can be provided by the oscillatory movement of telomere-bundled
354 chromosomes (Chacón et al., 2016; Takao et al., 2019). Additionally, noncoding RNAs
355 play a robust role in recognizing homologous pairs (Ding *et al.*, 2019; Ding et al., 2012).
356 Importantly, Rec8 dominates noncoding RNA-mediated robust pairing (Ding *et al.*,
357 2016a; Ding *et al.*, 2016b; Hiraoka, 2020). Therefore, Rec8-mediated chromatin
358 structures are an absolute requirement in the pairing homologous chromosomes during
359 meiosis.
360
361 **Loop-axis structure of chromatin in *S. pombe* meiosis**
362 Upon entry into meiosis in *S. pombe*, chromosomes form a loop between the Rec8 binding
363 sites (Figures 3B and S3B), which is also evident in *S. cerevisiae* meiosis (Muller et al.,
364 2018; Schalbetter *et al.*, 2019). Although this Rec8 geometry is undetectable via Hi-C in
365 mammalian meiosis (Luo et al., 2020; Patel *et al.*, 2019; Wang et al., 2019), it is argued
366 that the chromosomal position of Rec8 or loop location varies from one cell to another in
367 mammals (Patel *et al.*, 2019). Importantly, the Rec8 axis-loop structure formed normally
368 without LinEs in *S. pombe* (*rec10*Δ in Figure 3A). Therefore, we emphasize that the Rec8-
369 dependent axis-loop structure is distinct from LinEs and not a part of them. This
370 relationship seems to be valid between cohesin-dependent axis-loop structures and lateral
371 elements in other SC-forming organisms (Fujiwara *et al.*, 2020; Fukuda *et al.*, 2010;
372 Pelttari *et al.*, 2001). With the emergence of Rec8-dependent loop structures, TAD-like
373 signals observed in mitotic interphase cells mostly disappeared during meiotic prophase
374 (Figures 3A and 3E), similar to mammalian spermatocytes (Luo *et al.*, 2020; Patel *et al.*,

375 2019; Wang *et al.*, 2019). The emergence of a loop structure with the disappearance of
376 TADs is probably due to the switch of kleisin subunits from Rad21 to Rec8 that occurs
377 upon the commitment to meiosis.
378
379 Notably, in the meiotic prophase of *wpl1*Δ cells, the Rec8 axis became thicker, while each
380 chromatin loop became longer (Figures 4A, 4C, 4D, and 4E), as has been described in
381 mammalian somatic interphase cells (Haarhuis *et al.*, 2017). In the case of *S. cerevisiae*,
382 *WPL1* deletion was also reported to cause chromosomal compaction and recombination
383 defects with an increase in Rec8 amounts on chromatin (Challa *et al.*, 2016). If the axial
384 structures become thicker and the chromosomes become more compact, one would
385 intuitively expect that the alignment of homologs would be easier. However, the opposite
386 was true: X-shaped interactions tended to be reduced in the Hi-C analysis of *wpl1*Δ cells,
387 and alignment of chromosome arms also became defective in *wpl1*Δ (Figure S4F), similar
388 to *pds5*Δ (Ding *et al.*, 2016b). Pds5 associates with the cohesin complex and is required
389 for the chromosomal localization of Wpl1 (Ding *et al.*, 2006; Goto et al., 2017; Lin and
390 O'Connell, 2017), explaining the similar phenotypes of *pds5*Δ and *wpl1*Δ, such as thicker
391 Rec8 axis formation and the alignment of chromosome arms during meiosis (Figures 4A,
392 S4E, and S4F). These alignment defects are presumably caused by the overall stiffness of
393 the chromosomes with thicker axes in *wpl1*Δ. In fact, examination of the chromosomes
394 during horsetail movements in *wpl1*Δ rarely revealed torsional turning (Figure S4G,
395 Supplemental Movies 1, and 3). Thus, our findings imply an interesting mechanism by
396 which *S. pombe* maintains proper chromosome stiffness through the function of the Rec8
397 cohesin.
398

399 **Possible mechanisms for formation of the Rec8 chromatin axis**

400 The Rec8-dependent emergence of punctate Hi-C contacts only during meiosis suggests
401 mechanisms by which the chromatin loop structure is formed differently from mitotic
402 Rad21 cohesin. Fluorescence microscopy revealed that the Rec8 axis in the *wpl1*Δ
403 background is reproduced in the mutant of Rec10, Hop1 (a homolog of HORMAD), or
404 Mek1 (Figure S5J). All are required for LinE formation (Lorenz et al., 2006). The same
405 was true in the Rec12 mutant and regulators of Rec12, such as Rec7, Rec15, and Mei4
406 (Figures S5B and S5J). Our Hi-C analysis demonstrated that the chromatin loop structure
407 was also maintained in *rec10*Δ and *rec12*Δ (Figures 3A and S3A). Therefore, critical
408 regulators of Rec8 axis formation remain to be identified among the factors expressed in
409 a meiosis-specific manner and are required for recombination.

410

411 Mechanisms of chromatin loop formation have been proposed in mammalian somatic
412 cells. *cis*-Looping of distal chromatin or TAD formation is thought to be established by
413 the action of the Rad21 cohesin complex anchored on chromatin via the CCCTC-binding
414 factor (CTCF) (Li et al., 2020; Nora et al., 2017; Rao et al., 2014; Wutz et al., 2017).
415 More recently, a loop extrusion model was proposed for the formation of chromatin loops
416 by SMC protein complexes, including cohesin (Davidson and Peters, 2021; Fudenberg *et*
417 *al.*, 2016; Goloborodko et al., 2016; Sanborn *et al.*, 2015). In this model, the SMC protein
418 complex interacts with DNA, reels, and extrudes it through its own ring structure to form
419 a DNA loop (Davidson et al., 2019; Ganji et al., 2018; Kim et al., 2020; Kschonsak et al.,
420 2017; Terakawa et al., 2017). At least *in vitro*, human Rad21 cohesin is able to extrude
421 DNA, but it requires the cohesin loading factors Scc2 and Scc4 (Davidson *et al.*, 2019).
422 Interestingly, CTCF is a conserved factor only in vertebrates (Hore et al., 2008). Thus,

423 there are no homologs of CTCF in yeasts. In contrast, Scc2 and Scc4 are conserved from
424 yeasts to humans (Mis4 and Ssl3, respectively, in *S. pombe*). Interestingly, chromatin loop
425 structures were already observed in *S. pombe* at meiosis entry (0 h) when the Rec8 cohesin
426 is loaded by Mis4 and Ssl3 before pre-meiotic DNA replication (Figures 3A and S1A).
427 Furthermore, the *rec8-F204S* mutant isolated in this study showed a significant defect in
428 the formation of loop structures, despite maintaining the cohesion function. Strikingly,
429 phenylalanine at position 204 in Rec8 is located in the domain where kleisin interacts
430 with Scc2/Mis4, as previously shown by an *in vitro* binding assay (Kikuchi et al., 2016).
431 Thus, as an alternative scenario for an appealing molecular mechanism in the
432 establishment of meiosis-specific chromatin loop structures, Rec8 and Mis4 with Ssl3
433 may also play an important role. Mis4 with Ssl3 may replace the function of CTCF in
434 anchoring cohesin to chromatin. It is also plausible that some changes in chromatin may
435 have occurred upon entry into meiosis, such as the modification of histones suitable for
436 the formation of axes with chromatin loops by the Rec8 cohesin.
437
438 **Rec8 axis as a scaffold for LinE assembly**
439 In the *rec8-F204S* mutant, which was unable to form a loop structure, LinE formation
440 failed to occur and the recombination frequency was markedly reduced (Figures 7C, S7B,
441 and S7C). However, phosphorylation of Rec11, which is required for LinE formation,
442 was intact and the distribution of Rec8-F204S along the chromosomes was largely normal
443 (Figures 7B and S6B). Based on the observations of the localization of Rec10 (LinE) by
444 ChIP and fluorescence microscopy, Rec10 and Rec8 overlap in some regions of the
445 chromosome, but not in many other chromosome regions (Ding et al., 2021; Miyoshi *et*
446 *al.*, 2012; Sakuno and Watanabe, 2015). It is likely that the vast majority of Rec10 and

447 other LinE factors initially localize to chromosomes through interaction with Rec8
448 cohesin, and then are redistributed along the chromosome appropriately. We speculate
449 that the oligomerization of LinE factors, such as Rec10, is necessary for the formation of
450 LinE, which requires a certain amount of Rec8 to be present in a continuous axial
451 structure. The Rec8 axis acts as a scaffold to trigger the axial formation of LinEs.
452 Otherwise, LinE factors associated with the chromosome are not stabilized (Figure 7D).
453 As a result, LinE factors are released from the chromosome, and finally form aggregates
454 in the nucleus (Figures 7A, S7A, and 7D), due to their propensity to adhere to each other,
455 as in the polycomplex formed by mutants with defects in SC formation during meiosis of
456 *S. cerevisiae* (Zickler and Kleckner, 1999). Crucially, in addition to Rec11-5D mutant
457 protein, expression of the Rec11-Rec10 fusion protein, which can suppress the defects
458 caused by the loss of Rec11 phosphorylation (Sakuno and Watanabe, 2015), did not
459 suppress the LinE formation defect of *rec8-F204S* (Figures S7A, S7B and S7D). This
460 result strongly supports the view that the interaction between Rec8 and Rec10 is not
461 stabilized in the absence of the Rec8 axis along the chromatin. LinEs in *S. pombe* are
462 crucial in the assembly of complexes on chromatin that induce double-strand breaks on
463 DNA. This explains why a Rec8-dependent axis-loop structure is required for meiotic
464 recombination. Importantly, F204 in *S. pombe* Rec8 appears to be conserved among some
465 eukaryotes, including mammals. Although the relevant residue in mouse is leucine, we
466 demonstrated that the phenylalanine to leucine substitution in *S. pombe* Rec8 showed
467 almost no defects in axis formation (Figures 5D and S5I). Rec8 and Rec11/SA3 are
468 required for lateral element formation in mammals, as well as for axial element formation
469 in *S. pombe* (Fukuda *et al.*, 2014; Hopkins *et al.*, 2014; Llano *et al.*, 2014; Sakuno and
470 Watanabe, 2015; Winters *et al.*, 2014). Thus, there may be a mechanism by which

471 meiosis-specific cohesin-dependent axial structures can function as a scaffold in the
472 formation of lateral elements in mammals.
473
474 In conclusion, the current results obtained in *S. pombe* identify crucial functions of Rec8-
475 dependent assembly of chromatin structures that facilitate the execution of meiotic
476 recombination essential for faithful propagation of genetic materials into the progenies
477 during meiosis. The diverse and essential functions of the Rec8 cohesin in supporting
478 meiotic recombination may provide a basis for understanding the molecular mechanisms
479 of meiotic chromosome axis maturation and regulation of recombination in mammals,
480 potentially related to miscarriages and congenital abnormalities in humans (Nagaoka *et*
481 *al.*, 2012; Webster and Schuh, 2017).
482

483 **Acknowledgments**

484 We thank Drs. Masamitsu Sato, Shigehiro Kawashima and Juraj Gregan for providing
485 useful strains, Dr. Kayoko Tanaka for the helpful advice to induce highly synchronous
486 meiosis and all members of our laboratory for their valuable support and discussion. This
487 work was supported by JSPS KAKENHI grants JP26711020 (to T.S.), JP19K06503 (to
488 D.Q.D.), JP18H05528 (to T.H.), JP20H00454 and JP18H05533 (to Y.H.), and also by the
489 National Institutes of Health/National Institute of General Medical Sciences
490 (R01GM124195 to K.N.).
491

492 **Author contributions**

493 T.S., S.T., T.H., N.K., and Y.H. conceived and designed the experiments; T.S. conducted
494 almost all of the experiments except for the Hi-C, under supervision of T.H. and Y.H; S.T.

and O.I. performed Hi-C related analyses, under supervision of N.K; Bioinformatics-related works were implemented by H.T; D.-Q.D. provided the data about the pairing state in fission yeast meiosis; T.S., T.H., K.N., and Y.H. wrote the manuscript with the input from all the authors.

Declaration of interest

The authors declare no competing interests.

503 **Figure legends**

504 **Figure 1. Hi-C analysis firmly recapitulates the structure of meiotic bouquet**
505 **chromosomes**

506 (A) Chromosome arrangement in mitosis and meiosis in *S. pombe*. In mitosis (left),
507 centromeres are clustered at the spindle pole body (SPB) and display the Rabl orientation.
508 The grey lines indicate sister chromatids. In meiotic prophase (right), grey and black lines
509 indicate a homolog pair of chromosomes. Chromosomes are bundled by the telomeres
510 clustered at the SPB via telomeres, representing the bouquet orientation. (B) Hi-C contact
511 maps at 20 kbp resolution for three chromosomes prepared at vegetative growth (VG), 0
512 h, and 2.5 h after meiosis entry. Schematic views of each chromosome are shown on the
513 top and the left. Green arrowheads represent the centromere clustering. Blue arrowheads
514 in meiosis 0 h and 2.5 h represent the telomere clustering as depicted by the left lower
515 diagonal lines. The color scale on the right represents the percent ranking of contact
516 scores. (C) Heat maps showing the difference of contacts detected by Hi-C. Left,
517 subtraction of VG data from 0 h data. Right, subtraction of 0 h data from 2.5 h data. The
518 color scale on the right represents the percent ranking of difference scores. (D) Degree of
519 alignment of the two chromosome arms of telomere-bundled chromosome 1 is quantified
520 as the alignment index (Figure S1D) and is shown as the value along with a black vertical
521 line in the Hi-C contact map.

522

523 **Figure 2. Rec8 cohesin shapes chromosomes into a structure suitable for its**
524 **alignment**

525 (A) Hi-C contact maps of three chromosomes for the indicated strains, prepared from the
526 cells 0 h and 2.5 h after meiosis entry. The color scale on the right represents the percent

527 ranking of contact scores. (B) The alignment index for the indicated strains at meiotic
528 prophase (2.5 h after meiosis induction) is shown as the value along with a black vertical
529 line in the Hi-C contact map of chromosome 1.
530
531 **Figure 3. Rec8 cohesin is crucial to construct the meiosis-specific chromatin loops**
532 (A) Amplification of the Hi-C contact map in the 200 kbp region of chromosome 1 plotted
533 at 2 kbp resolution for the indicated strains at meiosis (0 h) and 2.5 h (at VG only for wild
534 type). The black arrow depicts the loop structure. (B) A merged view of the Hi-C contact
535 map and ChIP-chip data of Rec8 at the 200 kbp region of chromosome 1 shown in (A).
536 ChIP-chip data were adopted from the previously described source (Ito *et al.*, 2014). (C)
537 Contact probability versus genomic distance, *P(s)*, for VG (red), meiosis 0 h (blue) and
538 2.5 h (orange) of the wild type. The "shoulder" marked by the dotted line at approximately
539 50 kbp represents an increase in interactions within a region shorter than that length. (D)
540 Contact probability versus genomic distance, *P(s)*, for wild type (red), *rec8*Δ (blue),
541 *rec10*Δ (orange), and *rec12*Δ (green) 2.5 h after meiotic induction. (E) Amplification of
542 Hi-C contact maps at the 500 kbp region of chromosome 1and 2 plotted at 5 kbp
543 resolution for wild type strain at VG, meiosis 0 h and 2.5 h. The dotted line depicts the
544 TAD-like structure. (F) Schematic diagram of chromosome conformation at meiotic
545 prophase in *S. pombe*. All chromosomes are tightly aligned from the telomeres to the
546 centromeres. Rec8 establishes the meiosis-specific chromatin loop structure, irrespective
547 of LinEs or recombination.
548
549 **Figure 4. Wpl1 regulates chromatin loop length during meiotic prophase in *S. pombe***
550 (A) Serial Z sections (0.3 μm each) of Rec8-GFP signals at meiotic prophase in wild type

551 and *wpl1*Δ. Axis-like signals of Rec8 are clearly observed in *wpl1*Δ. (B) Upper panel
552 displays Hi-C contact maps of three chromosomes at 20 kbp resolution in *wpl1*Δ at
553 vegetative growth (VG) and 0 h, and 2.5 h after meiosis entry, with schematic views of
554 each chromosome. The color scale on the right represents the percent ranking of contact
555 scores. The lower panel displays heat maps showing the difference of contacts detected
556 in each genome region by Hi-C in wild type and *wpl1*Δ at VG, and meiosis 0 h and 2.5 h.
557 The color scale on the right represents the percent ranking of difference scores. (C)
558 Amplification of Hi-C contact maps showing the 200 kbp region of chromosome 2 plotted
559 at 2 kbp resolution for the indicated strains at VG and meiosis 0 h and 2.5 h. (D) *P(s)*s for
560 meiosis 0 h and 2.5 h of wild type (red and blue) and *wpl1*Δ (orange and green). The blue
561 or green dotted line represent a shoulder of wild type or *wpl1*Δ at 2.5 h after meiosis entry,
562 respectively. (E) The number of loops per chromatin distance in *wpl1*Δ and wild type was
563 calculated. The value obtained by dividing *wpl1*Δ data by wild type data is shown as the
564 $\log_2$ ratio.
565
566 **Figure 5. Isolation of *rec8* mutant showing defect in axis formation with intact**
567 **cohesion function**
568 (A) The left panel shows a schematic view of cohesin complexes in fission yeast in
569 mitosis and meiosis. In mitosis, Rad21-Psc3 cohesin complex ubiquitously locates along
570 the whole chromosomes. In meiosis, Rec8-Psc3 cohesin complex exists only at the
571 centromeres and Rec8-Rec11 cohesin complex at the chromosomal arm regions. The
572 right panel shows the scheme for isolation of *rec8* mutants that specifically show defects
573 in axis formation, but normal cohesion in meiotic prophase. The promoter of the *rec8*
574 gene is replaced by the *adh1* promoter, and the promoter of the *rec11* gene is replaced by

575 the *adh41* (a weaker version of *adh1*) promoter, to allow their expression both in mitosis
576 and meiosis. After transformation of a library of GFP-fused *rec8* mutants with a selective
577 marker *bsdR* (not shown here), the obtained blasticidin-resistant colonies were
578 subsequently induced to meiosis to observe the axial Rec8-GFP signals. Growth rate of
579 the blasticidin-resistant clone acts as an indicator of the functionality of Rec8-Rec11
580 cohesin. (B) Representative pictures of Rec8-GFP with a cell shape (white dotted line)
581 during meiotic prophase in wild type and the isolated *rec8-F204S* mutant in this screening.
582 (C) Cohesion defects in the chromosome arm region (*cut3*$^{+}$ locus, left arm of chromosome
583 2) were examined in the indicated cells arrested at prophase I by the *mei4*Δ mutation.
584 After fixation by methanol, the number of heterozygous *cut3*-GFP signals was counted
585 (n > 150). A score of 2 or 1.5 *cut3*-GFP signals represents the complete or partial loss of
586 sister chromatid cohesion, respectively. The *rec8-S552P* identified in this screening
587 displays a remarkable defect in cohesion that is stronger than that of *rec8*Δ (see the text).
588 Error bars show standard deviations (SD) from three independent experiment. P values
589 were obtained from Chi-square test for statistical significance. (D) The upper panel is a
590 schematic diagram of *S. pombe* Rec8. Domains for the known interaction with cohesin-
591 related factors are shown. The position of F204 is also indicated by the red arrowhead.
592 The lower panel depicts the alignment of Rec8 homologs in *Shizosaccharomyces pombe*
593 (Sp), *S. octosporus* (So), human (h), mouse (m) and frog (*Xenopus leaves*) (x). (E) Time-
594 lapse observation (5 min intervals) of horsetail nuclear movement in the indicated cells
595 stained with histone H2B-mCherry. The right cartoon represents a model of the chromatin
596 state for each strain. In *rec8*Δ, Rad21 partially compensates the cohesion defect. (F) The
597 upper left panel shows a schematic drawing of the distance of *ade8-lacO* inserts from the
598 telomere of chromosome II. The upper right panels represent images of GFP signals for

599 the indicated strains. Brighter GFP signals at the edge of nucleus represent telomeres
600 (Taz1-GFP) and weaker GFP signals represent the *ade8* locus. The lower graph displays
601 a plot of the distance between the telomere and the *ade8* locus in each cell during meiotic
602 prophase for the indicated strains with average distance (n=55).
603

604 **Figure 6. *rec8-F204S* mutant displays defective chromatin loop formation**

605 (A) Hi-C contact maps of three chromosomes at 20 kbp resolution in wild type *rec8*-3×Pk
606 and *rec8-F204S*-3×Pk cells at 0 h and 2.5 h after meiosis entry, with schematic views of
607 each chromosome. The color scale on the right represents the percent ranking of contact
608 scores. (B) The alignment index for indicated strains at meiotic 0 h and 2.5 h after meiosis
609 induction is shown as the value along with a black vertical line in the Hi-C contact map
610 of chromosome 1. (C) Amplification of Hi-C contact maps of the 200 kbp region of
611 chromosome 1 (upper) and chromosome 2 (lower) at 2 kbp resolution, for the indicated
612 strain at meiosis 0 h and 2.5 h. (D) Contact probability versus genomic distance, *P(s)*, for
613 meiosis 0 h and 2.5 h of *rec8-wt* (red and blue) and *rec8-F204S* (orange and green). A
614 shoulder observed in meiosis 2.5 h of *rec8-wt* was shown with dotted line. (E) Number
615 of each loop per length quantified using genome-wide loop caller HiCCUPS for the
616 indicated strains at meiosis 0 h (left) and 2.5 h (right).
617

618 **Figure 7. Rec8-dependent chromatin loop formation and meiotic recombination**

619 (A) Representative pictures of Rec10-mCherry with cell shape (white dotted line) during
620 meiotic prophase for the indicated strains. The yellow arrows depict the aggregates of
621 LinE. (B) Western blot analysis. Whole-cell extracts were prepared from meiotic
622 prophase (2.5 h after meiosis induction) expressing Rec8-3×Flag in wild type and *rec8-*

623 *F204S,* with Psm1-3×HA. Rec11 phosphorylation by CK1 was detected by anti-
624 phosphorylated Rec11 (at T7). The monoclonal anti-tubulin (DM1A, Abcam) antibody
625 was used as a loading control. (C) Intergenic meiotic recombination for *ura1-lys3* (n >
626 700), *cox7-vps38* (n > 500), and *vps38-leu1* (n > 500) in the indicated zygotes. Error bars
627 show standard deviations (SD) from three independent experiment. (D) Model for the
628 Rec8 cohesin-dependent regulation of LinE assembly and meiotic recombination. After
629 the commitment in meiosis, Rec8 cohesin shown in blue is loaded onto the chromosomes
630 via cohesin loader complex (Mis4-Ssl3) shown in orange. Once loaded, Rec8 cohesin
631 promotes the loop formation that is antagonized by Wpl1 shown by purple. By meiotic
632 prophase, in parallel with the continuous loading of Rec8 and phosphorylation of Rec11
633 by CK1 (indicated by red triangles), chromatin looping with axis formation by Rec8
634 cohesin occurs to form chromatin to recruit LinE factors. See the detailed description in
635 the Discussion.
636

637 **STAR Methods**

638 ***S. pombe* strains**

639 All media and growth conditions were as described previously (Moreno et al., 1991).
640 Complete medium supplemented with uracil, lysine, adenine, histidine, and leucine
641 (YE5S), minimal medium (EMM2), and sporulation-inducing medium (SPA and SSA)
642 were used unless otherwise stated. The strains used in this study are listed in Table S1.
643 Deletion of the endogenous genes (*rec12*$^{+}$, *rec11*$^{+}$, *rec7*$^{+}$, *rec15*$^{+}$, *mek1*$^{+}$, *rec8*$^{+}$, *rec10*$^{+}$,
644 *hop1*$^{+}$, *wpl1*$^{+}$, *pds5*$^{+}$, and *mei4*$^{+}$) and tagging (*rec10*$^{+}$, *rec8*$^{+}$, *psm1*$^{+}$, *rec25*$^{+}$, *rad21*$^{+}$, and
645 *rec11*$^{+}$) using GFP, mCherry, 3×hemagglutinin (HA) tag, 3×Pk (V5 tag), or 3×Flag was
646 performed according to the PCR-based gene targeting method for *S. pombe* using the
647 *ura4*$^{+}$, *kanMX6 (kanR), hphMX6 (hygR), natMX6 (natR)*, and *bsdR* genes as selection
648 markers (Bahler et al., 1998; Rabitsch et al., 2001; Sato et al., 2005). Histone H2B tagging
649 by mCherry for time-lapse observation has been described previously (Ruan et al., 2015).
650 The CK1 shut off mutant, *rec11-5A* mutant, *rec11-5D* mutant, and the strain expressing
651 Rec10-GFP-Rec11 fusion protein have been described previously (Sakuno and Watanabe,
652 2015). For the assay of crossing over recombination frequency, the *hygR* cassette was
653 inserted 1215 bp upstream from the start codon of the *cox7*$^{+}$ gene and the *natR* cassette
654 was inserted 1000 bp upstream from the start codon of *vps38*$^{+}$ gene using the PCR-based
655 gene targeting method. To generate strains of *rec8* point mutants with tagging of GFP or
656 3×Pk tag, the endogenous *rec8*$^{+}$ locus was cloned with its promoter and terminator into
657 pUC119. Using the NEBuilder system (New England Biolabs), a DNA fragment encoding
658 GFP or 3×Pk tag with *kanR or bsdR* was introduced immediately before the stop codon
659 of the *rec8* gene cloned in pUC119. Next, target sequences of *rec8*$^{+}$ were subsequently
660 mutated using the KOD One Master Mix Blue (TOYOBO) to generate an amino acid

661 substitution. In case of *rec8-S552P*, a C-terminal portion of *rec8*$^{+}$ open reading frame
662 including the mutation site and marker gene with the *rec8*$^{+}$ terminator was amplified by
663 PCR and transformed into the wild type *rec8*$^{+}$ locus. Alternatively, in the case of N-
664 terminal mutations such as *rec8-F204S*, the promoter to terminator of the *rec8*$^{+}$ gene,
665 including the mutation and marker gene, was amplified by PCR and transformed into the
666 Δ*rec8::ura4*$^{+}$ strain. Correct replacement was confirmed using PCR and direct
667 sequencing. The strain in which the mitotic cohesin, Rad21 and Psc3, were exchanged
668 for meiotic cohesin (Rec8 and Rec11) has been described previously (Kitajima *et al.*,
669 2003). To construct the *pat1-as2* diploid with MDR-sup, haploid strains (*h*$^{-}$ *pat1-as2*
670 *MDR-sup* and *h*$^{-}$ *pat1-as2 MDR-sup mat-Pc*) were used (they were generously provided
671 by Masamitsu Sato, Waseda University). After introducing tagging or disruption of a gene
672 of interest in both haploids, protoplast fusion was performed as described previously
673 (Flor-Parra et al., 2014), except for the use of Lysing Enzyme (Sigma-Aldrich) instead of
674 Lallzyme or Zymolyase.
675

676 **Preparation of meiotic cells**

677 For microscopic observation of Rec8-GFP, Rec11-GFP, Rec10-mCherry, and Rec25-
678 mCherry, *h*^{90} cells cultured on YE plates at 26°C overnight were streaked on SSA plates,
679 or suspended in 20 mg/ml of leucine and spotted on SPA or SSA plates. The cells were
680 incubated at 26°C for 6–10 h to observe the cells at the horsetail stage. In case of
681 *lacO*/lacI-GFP observation for cohesion assays (Figure 5C and S5D), *h*$^{+}$ and *h*$^{-}$ cells were
682 mixed with 20 mg/ml of leucine and spotted on SSA or SPA plates. For the
683 immunoprecipitation of Rec8-GFP with Psm1-3HA (Figures S5F), *h*$^{+}$/*h*$^{-}$ diploid cells
684 with *mei4*Δ were used to arrest the cells at the meiotic prophase. In the case of diploid

685 cells, the cells were grown in EMM2 liquid medium containing 5 mg/ml NH_4Cl at a
686 density of 5×10^6 cells/ml at 25°C and then resuspended in EMM2 (1% glucose) medium
687 lacking NH_4Cl at a density of 1×10^7 cells/ml at 25°C for 15 h. For the
688 immunoprecipitation of Rec8-3×Flag with Psm1 (Figure S5G), ChIP assay (Figure S6B),
689 detection of phosphorylated Rec11 (Figure 7B), and Hi-C analyses, we used h^-/h^- diploid
690 cells with *pat1-as2* and *MDR-sup* alleles. Cells grown in YE liquid medium at a density
691 of $5–10\times10^6$ cells/ml at 25°C were collected by centrifugation and washed twice with
692 EMM2 (1% glucose) medium lacking NH_4Cl (EMM2-N). Cells were then resuspended
693 in EMM2-N with 50 mg/ml leucine at a density of 5×10^6 cells/ml and incubated at 25℃
694 for 6.5 h to induce G1 arrest. By adding the same volume of EMM2-N with 50 mg/ml
695 leucine and 15 μM of 1-NM-PP1 (Toronto Research Chemicals Inc.) ($5–8\times10^6$ cells/ml),
696 cells can enter meiosis. They were further incubated for 2.5 h or more. Before harvesting
697 the meiotic cells, 1 mM phenylmethylsulfonyl fluoride (PMSF; Sigma-Aldrich) was
698 added to reduce protein degradation.
699
700 **Rec8 mutant screening**
701 The *rec8*$^+$ cDNA mutant library used for the screening was constructed as follows. The
702 DNA region encoding *3×HA-ura4*$^+$of the plasmid VP068 (pUC119 base, *Padh1-*
703 *rec8*$^+$cDNA-*3×HA-ura4*$^+$*-Trec8*) (Yokobayashi *et al.*, 2003) was replaced by the DNA
704 region encoding GFP-BsdR to produce VP068-GFP-bsd. Error-prone PCR of *rec8*$^+$
705 cDNA in VP068-GFP-BsdR by Ex taq (TaKaRa Bio) was performed using several
706 concentrations of $MnCl_2$ (final 0.05 mM, 0.15 mM, 0.25 mM, and 0.3 mM) and an
707 additional 1 mM dGTP or dATP with 0.2 mM of dNTP mix (total 8 conditions). By using
708 the NEBuilder system, amplified *rec8*$^+$cDNA pools (from eight conditions) were then

709 cloned into the fragment, which was amplified by inverse PCR of VP068-GFP-BsdR
710 without the *rec8*$^{+}$ cDNA region. In total, approximately 5300 *Escherichia coli*
711 transformants (representing library size) were generated. All colonies were recovered
712 from the plates, and plasmids (pRec8 library) were extracted. The pRec8 library was
713 estimated to contain approximately six mutations/kb. Using the pRec8 library as a
714 template, the region from 620 bp upstream of the *adh1*$^{+}$ promoter to 600 bp downstream
715 of the *rec8*$^{+}$ terminator was amplified by PCR. These fragments were used to transform
716 the screening host strains. More than 95% of blasticidin-resistant colonies obtained after
717 transformation showed correct integration, as confirmed by PCR. Rec8-GFP signals
718 during meiotic prophase were observed among the blasticidin-resistant colonies, which
719 showed relatively normal growth.
720
721 **Fluorescence microscopy**
722 Fluorescence images were obtained using an Axioplan2 microscope (Carl Zeiss)
723 equipped with a Quantix cooled CCD camera (Photometrics) and a DeltaVision
724 microscope system (GE Healthcare Inc.) equipped with a CoolSNAP HQ2 cooled CCD
725 camera (Photometrics) and a 60× Plan-ApoN SC oil immersion objective lens (NA=1.40;
726 Olympus). The brightness of the images was adjusted using Fiji software (Schindelin et
727 al., 2012) without changing the gamma settings. The pairing frequency was quantified as
728 described previously (Ding et al., 2004).
729 For time-lapse live-cell imaging of Rec8-GFP and H2B-mCherry, cells were
730 cultured overnight in liquid EMM2 at 26°C to reach stationary phase, and cells were
731 spotted onto SPA plates to induce meiosis, and incubated at 26°C for 4–5 h. Zygotes
732 suspended in 1% glucose EMM2 (1% glucose) without nitrogen were sonicated briefly

733 and immobilized on a coverslip coated with lectin in a 35 mm glass-bottomed culture dish
734 (MatTek) and observed at 26°C in liquid EMM2 (1% glucose) without nitrogen using a
735 DeltaVision microscope in an air-conditioned room. Images were collected at
736 approximately nine focal sections with 0.45 μm interval at each time point. The images
737 were collected every 5 min at three focal sections to minimize the excitation light during
738 long-term observation. Images were subsequently acquired using Z-sectioning and
739 projected according to the SoftWoRx software program (Applied Precision).
740

741 **Immunoprecipitation**

742 The cell extracts (~8×10^7 cells) were prepared by bead-beating cells in IP buffer (50 mM
743 HEPES-KOH at pH 8.0, 150 mM NaCl, 1 mM dithiothreitol, 2.5 mM $MgCl_2$, 20%
744 glycerol, 1 mM PMSF, 0.8% Triton X-100, 0.1% sodium deoxycholate, and 5× protease
745 inhibitor cocktail (P8215; Sigma-Aldrich). Fifty units of DNase I (TaKaRa Bio) were
746 added to the cell extract and sonicated (Branson Inc.). After collecting the supernatant as
747 whole-cell extracts by centrifugation at 15,00 rpm for 30 min, immunoprecipitation was
748 performed by incubating these extracts for 1 h at 4°C with anti-GFP polyclonal antibodies
749 (Rockland) or anti-Flag polyclonal antibodies (anti-DDDDK, MBL), and an additional 2
750 h at 4°C with 20 μl of a slurry of IgG-conjugated dynabeads (Invitrogen). After washing
751 the beads five times with IP buffer, the whole-cell extracts and immunoprecipitates were
752 subjected to western blotting using monoclonal anti-GFP (JL-8, Roche), Flag-M2
753 monoclonal antibody (Sigma-Aldrich), monoclonal anti-HA (3F10, Roche), and
754 monoclonal anti-tubulin (DM1A, Abcam) antibodies.
755

756 **ChIP assay**

757 The procedures were carried out as described previously (Yokobayashi and Watanabe,
758 2005). Anti-FLAG M2 monoclonal antibody (Sigma-Aldrich) and IgG conjugated
759 dynabeads (Invitrogen) were used for immunoprecipitation. DNA prepared from the
760 whole-cell extracts or immunoprecipitated fractions was analyzed via quantitative PCR
761 (qPCR) with the StepOnePlus Real-Time PCR system (Thermo Fisher Scientific) using
762 Power SYBR Green PCR Master Mix© Green I Master (Thermo Fisher Scientific). The
763 primers used for PCR have been described previously (Sakuno and Watanabe, 2015).
764 Immunoprecipitation with control mouse IgG antibody (Abcam) was performed in each
765 experiment to account for nonspecific binding in the ChIP fractions and verify the
766 significance of immunoprecipitation. The percent IP was quantified using three
767 independent qPCR experiments.
768
769 **Recombination assay**
770 For intergenic recombination, haploid strains containing appropriate markers were mated
771 and sporulated at 26°C on SSA plates for 30 h. The spores were isolated using β-
772 glucuronidase solution (Wako) and plated on YE. The colonies were then replicated in
773 selective media [EMM2-uracil, EMM2-lysine, EMM2-lysine, YE5S containing
774 hygromycin B (FUJIFILM) or YE5S containing clonNAT (WERNER BioAgents)] and
775 YE5S containing phloxine B (Wako) to select haploid cells. In the *ura1-lys3* interval, the
776 degree of lysine auxotrophy among the uracil prototrophic colonies (n>700, replicated
777 three times) was assessed. In the *cox7*$^{+}$-*vps38*$^{+}$ interval, the degree of hygromycin B-
778 resistant (*hygR*-containing) colonies among the clonNAT-resistant (*natR*-containing)
779 colonies was assessed (n>500, and replicated three times). In the *vps38*$^{+}$-*leu1*$^{+}$ interval,
780 the degree of leucine prototrophic colonies among the clonNAT-resistant (*natR*-

781 containing) colonies was assessed (n>500, and replicated three times). For intragenic
782 recombination, h^{90} haploid strains containing the *ade6-M26* allele and plasmids harboring
783 the *ade6-469* allele according to the $ura4^{+}$ marker (Ponticelli and Smith, 1992) were
784 sporulated at 26°C on SPA plates for 30 h. The spores were isolated by treatment with
785 glusulase and plated on YE5S containing phloxine B (to count all viable haploid spores)
786 and EMM2-adenine plates. The frequency of intragenic recombination was quantified as
787 the degree of adenine prototrophic colonies among viable haploid spores (n>7400, and
788 replicated three times).
789
790 **Flow cytometry**
791 A total of 1×10^{7} cells were fixed with 70% ethanol and incubated with 50 µg/ml RNase
792 A in 500 µl of 50 mM sodium citrate (pH 7.5) for 4 h at 37°C, and then stained with 0.5
793 µg/ml propidium iodide. DNA content of 1.5×10^{5} cells was measured on a FACS Calibur
794 instrument (BD Biosciences).
795
796 **In situ Hi-C**
797 In situ Hi-C experiments were performed as described previously (Tanizawa *et al.*, 2017)
798 with minor modifications. Asynchronous or meiotic cell cultures of 4×10^{8} cells were
799 fixed with 3% paraformaldehyde at 26°C for 10 min. The fixed cells were disrupted using
800 glass beads and Mini-Beadbeater-16 (BioSpec Products) in lysis buffer (50 mM
801 HEPES/KOH pH 7.5, 140 mM NaCl, 1 mM EDTA, 1% Triton X-100, 0.1% sodium
802 deoxycholate, 1× Complete [Roche, 11836170001], and 1 mM PMSF). The lysed cells
803 were collected by centrifugation and permeabilized by resuspension with 1.11× NEBuffer
804 2 (B7002, NEB) containing 0.1% sodium dodecyl sulfate (SDS) at 62°C for 7 min. After

805 SDS was quenched by adding 1/9 volume of 10% Triton X-100, the permeabilized cells
806 were treated with 25 units of MboI (R0147, NEB) at 37°C overnight. The enzyme was
807 inactivated by incubation at 62°C for 20 min. After centrifugation, the pellet containing
808 the restricted DNA fragments was used in the following procedure. A half volume of fill-
809 in mix [1× NEBuffer 2, 150 μM biotin-14-dATP (NU-835-BIO14, Jena Bioscience), 150
810 μM dCTP, 150 μM dGTP, 150 μM dTTP, 0.4 units/μL Klenow fragment (M0210, NEB)]
811 was added to the pellet and incubated at 37°C for 45 min. Subsequently, three volumes
812 of ligation mix [1.33× T4 DNA ligase buffer (B0202, NEB), 1.11% Triton X-100, 133
813 μg/ml bovine serum albumin (B9001, NEB), 5.56 units/μl T4 DNA ligase (M0202,
814 NEB)] was added and incubated at room temperature (~25°C) for 4 h. After ligation, the
815 pellet was collected by centrifugation, resuspended in proteinase K solution [10 mM Tris-
816 HCl pH 8.0, 200 mM NaCl, 1 mM EDTA, 0.5% SDS, 0.5 mg/ml proteinase K (25530049,
817 Invitrogen)], and incubated at 65°C overnight. DNA was purified by phenol-chloroform
818 treatment followed by ethanol precipitation, and then fragmented by sonication with a
819 model UCD-200 Bioruptor (Diagenode). After the biotin-labeled DNA was pulled down
820 with Dynabeads Streptavidin T1 (65601, Invitrogen), the beads were washed twice with
821 TNB (5 mM Tris-HCl pH 7.5, 0.5 mM EDTA, 1 M NaCl, 0.05% Tween-20) at 55°C for
822 2 min. To ligate the Illumina sequencing adaptors to the biotinylated DNA fragments, the
823 beads were successively treated with end repair mix [1× T4 DNA ligase buffer, 1 mM
824 dATP, 0.5 mM each dNTP, 0.5 units/μl T4 polynucleotide kinase (M0201, NEB), 0.12
825 units/μl T4 DNA polymerase (M0203, NEB), 0.05 units/μl Klenow fragment] at 25°C for
826 30 min, dA-tailing mix [1× NEBuffer 2, 0.5 mM dATP, 0.25 units/μl Klenow exo-
827 (M0212, NEB)] at 37°C for 30 min, and Illumina adaptor ligation mix [0.075x End repair
828 reaction buffer (E6050, NEB), 0.32× Ligation master mix (E7595, NEB), 0.011× Ligation

829 enhancer, and 45 nM NEBNext adaptor for Illumina] at 20°C for 15 min followed by
830 0.032 units/µl USER treatment at 37°C for 15 min, with two washes with TNB at 55°C
831 for 2 min after each reaction. The resultant adaptor-ligated Hi-C library was amplified by
832 PCR with five to seven cycles with Q5 master mix (M0544, NEB) and index primers
833 (E7335/E7500/E7710/E7730, NEB) before 37 bp paired-end sequencing using the
834 NextSeq 500 device (Illumina).
835
836 **In situ Hi-C data analysis**
837 In situ Hi-C data were processed as described previously (Tanizawa *et al.*, 2017). The
838 paired reads were separately aligned to the fission yeast genome (version ASM294v2.19)
839 using Bowtie2 (version 2.2.9) with the iterative alignment strategy. The aligned reads
840 were assigned to MboI fragments. Redundant paired reads derived from PCR biases,
841 aligned to repetitive sequences, or with low mapping quality (MapQ < 30) were removed.
842 Paired reads potentially derived from self-ligation and undigested products were also
843 discarded.
844 The fission yeast genome was divided into non-overlapped 20-kb, 5-kb, or 2-
845 kb bins. Raw contact matrices were constructed by counting paired reads assigned to two
846 bins, and Hi-C biases in the contact matrices were corrected using the ICE method
847 (Imakaev et al., 2012). The ICE normalization was repeated 30 times. ICE-normalized
848 contact scores were used for all heat maps, where the maximum intensity corresponded
849 to the top 5% score. For subtraction heat maps, the top 5% absolute values of difference
850 scores (T) were extracted. The T and $-T$ scores were drawn as the maximum and minimum
851 intensity.
852

Loop detection

Knight and Ruiz (KR) normalized matrices (Rao *et al.*, 2014) in .hic format was calculated from raw contact matrices using the 'pre' function of Juicer_tools (version 1.22.01) (Durand et al., 2016). Loop calling was performed for KR-normalized matrices using HiCCUPS ('hiccups' function of Juicer_tools) with the following parameters: r 2000 -k KR -f .01 -p 3 -i 7 -d 10000".

References

Aoi, Y., Sato, M., Sutani, T., Shirahige, K., Kapoor, T.M., and Kawashima, S.A. (2014). Dissecting the first and the second meiotic divisions using a marker-less drug-hypersensitive fission yeast. Cell Cycle *13*, 1327-1334. 10.4161/cc.28294.

Bahler, J., Wu, J., Longtine, M.S., Shah, N.G., McKenzie III, A., Steever, A.B., Wach, A., Philippsen, P., and Pringle, J.R. (1998). Heterologous modules for efficient and versatile PCR-based gene targeting in *Schizosaccharomyces pombe*. Yeast *14*, 943-951.

Bähler, J., Schuchert, P., Grimm, C., and Kohli, J. (1991). Synchronized meiosis and recombination in fission yeast: observations with pat1-114 diploid cells. Curr Genet *19*, 445-451. 10.1007/BF00312735.

Bähler, J., Wyler, T., Loidl, J., and Kohli, J. (1993). Unusual nuclear structures in meiosis prophase of fission yeast : a cytological analysis. J. Cell Biol. *121*, 241-256.

Cai, X., Dong, F., Edelmann, R.E., and Makaroff, C.A. (2003). The Arabidopsis SYN1 cohesin protein is required for sister chromatid arm cohesion and homologous chromosome pairing. Journal of cell science *116*, 2999-3007.

Chacón, M.R., Delivani, P., and Tolić, I.M. (2016). Meiotic Nuclear Oscillations Are Necessary to Avoid Excessive Chromosome Associations. Cell Rep *17*, 1632-1645. 10.1016/j.celrep.2016.10.014.

Challa, K., Lee, M.S., Shinohara, M., Kim, K.P., and Shinohara, A. (2016). Rad61/Wpl1 (Wapl), a cohesin regulator, controls chromosome compaction during meiosis. Nucleic Acids Res *44*, 3190-3203. 10.1093/nar/gkw034.

Challa, K., Shinohara, M., and Shinohara, A. (2019). Meiotic prophase-like pathway for cleavage-independent removal of cohesin for chromosome morphogenesis. Curr Genet *65*, 817-827. 10.1007/s00294-019-00959-x.

Chikashige, Y., Ding, D.Q., Funabiki, H., Haraguchi, T., Mashiko, S., Yanagida, M., and Hiraoka, Y. (1994). Telomere-led premeiotic chromosome movement in fission yeast. Science *264*, 270-273. 10.1126/science.8146661.

Chikashige, Y., Ding, D.Q., Imai, Y., Yamamoto, M., Haraguchi, T., and Hiraoka, Y. (1997). Meiotic nuclear reorganization: switching the position of centromeres and telomeres in the fission yeast Schizosaccharomyces pombe. EMBO J *16*, 193-202. 10.1093/emboj/16.1.193.

Cipak, L., Hyppa, R.W., Smith, G.R., and Gregan, J. (2012). ATP analog-sensitive Pat1 protein kinase for synchronous fission yeast meiosis at physiological temperature. Cell Cycle *11*, 1626-1633. 10.4161/cc.20052.

Crawley, O., Barroso, C., Testori, S., Ferrandiz, N., Silva, N., Castellano-Pozo, M., Jaso-Tamame, A.L., and Martinez-Perez, E. (2016). Cohesin-interacting protein WAPL-1 regulates meiotic chromosome structure and cohesion by antagonizing specific cohesin complexes. Elife *5*, e10851. 10.7554/eLife.10851.

Davidson, I.F., Bauer, B., Goetz, D., Tang, W., Wutz, G., and Peters, J.M. (2019). DNA loop extrusion by human cohesin. Science *366*, 1338-1345. 10.1126/science.aaz3418.

Davidson, I.F., and Peters, J.M. (2021). Genome folding through loop extrusion by SMC complexes. Nat Rev Mol Cell Biol *22*, 445-464. 10.1038/s41580-021-00349-7.

Davis, L., Rozalen, A.E., Moreno, S., Smith, G.R., and Martin-Castellanos, C. (2008). Rec25 and Rec27, novel linear-element components, link cohesin to meiotic DNA breakage and recombination. Curr Biol *18*, 849-854. 10.1016/j.cub.2008.05.025.

Ding, D.Q., Chikashige, Y., Haraguchi, T., and Hiraoka, Y. (1998). Oscillatory nuclear movement in fission yeast meiotic prophase is driven by astral microtubules, as revealed by continuous observation of chromosomes and microtubules in living cells. J Cell Sci *111 (Pt 6)*, 701-712.

Ding, D.Q., Haraguchi, T., and Hiraoka, Y. (2016a). A cohesin-based structural platform supporting homologous chromosome pairing in meiosis. Curr Genet *62*, 499-502. 10.1007/s00294-016-0570-x.

Ding, D.Q., Matsuda, A., Okamasa, K., and Hiraoka, Y. (2021). Linear elements are stable structures along the chromosome axis in fission yeast meiosis. Chromosoma. 10.1007/s00412-021-00757-w.

Ding, D.Q., Matsuda, A., Okamasa, K., Nagahama, Y., Haraguchi, T., and Hiraoka, Y. (2016b). Meiotic cohesin-based chromosome structure is essential for homologous chromosome pairing in Schizosaccharomyces pombe. Chromosoma *125*, 205-214. 10.1007/s00412-015-0551-8.

Ding, D.Q., Okamasa, K., Katou, Y., Oya, E., Nakayama, J.I., Chikashige, Y., Shirahige, K., Haraguchi, T., and Hiraoka, Y. (2019). Chromosome-associated RNA-protein complexes promote pairing of homologous chromosomes during meiosis in Schizosaccharomyces pombe. Nat Commun *10*, 5598. 10.1038/s41467-019-13609-0.

Ding, D.Q., Okamasa, K., Yamane, M., Tsutsumi, C., Haraguchi, T., Yamamoto, M., and Hiraoka, Y. (2012). Meiosis-specific noncoding RNA mediates robust pairing of homologous chromosomes in meiosis. Science *336*, 732-736. 10.1126/science.1219518.

Ding, D.Q., Sakurai, N., Katou, Y., Itoh, T., Shirahige, K., Haraguchi, T., and Hiraoka, Y. (2006). Meiotic cohesins modulate chromosome compaction during meiotic prophase in fission yeast. J Cell Biol *174*, 499-508. jcb.200605074 [pii] 10.1083/jcb.200605074.

Ding, D.Q., Yamamoto, A., Haraguchi, T., and Hiraoka, Y. (2004). Dynamics of homologous chromosome pairing during meiotic prophase in fission yeast. Dev Cell *6*, 329-341. 10.1016/s1534-5807(04)00059-0.

Durand, N.C., Shamim, M.S., Machol, I., Rao, S.S., Huntley, M.H., Lander, E.S., and Aiden, E.L. (2016). Juicer Provides a One-Click System for Analyzing Loop-Resolution Hi-C Experiments. Cell Syst *3*, 95-98. 10.1016/j.cels.2016.07.002.

Estreicher, A., Lorenz, A., and Loidl, J. (2012). Mug20, a novel protein associated with linear elements in fission yeast meiosis. Curr Genet *58*, 119-127. 10.1007/s00294-012-0369-3.

Flor-Parra, I., Zhurinsky, J., Bernal, M., Gallardo, P., and Daga, R.R. (2014). A Lallzyme MMX-based rapid method for fission yeast protoplast preparation. Yeast *31*, 61-66. 10.1002/yea.2994.

Fudenberg, G., Imakaev, M., Lu, C., Goloborodko, A., Abdennur, N., and Mirny, L.A. (2016). Formation of Chromosomal Domains by Loop Extrusion. Cell Rep *15*, 2038-2049. 10.1016/j.celrep.2016.04.085.

Fujiwara, Y., Horisawa-Takada, Y., Inoue, E., Tani, N., Shibuya, H., Fujimura, S., Kariyazono, R., Sakata, T., Ohta, K., Araki, K., et al. (2020). Meiotic cohesins mediate initial loading of HORMAD1 to the chromosomes and coordinate SC formation during meiotic prophase. PLoS Genet *16*, e1009048. 10.1371/journal.pgen.1009048.

Fukuda, T., Daniel, K., Wojtasz, L., Toth, A., and Höög, C. (2010). A novel mammalian HORMA domain-containing protein, HORMAD1, preferentially associates with unsynapsed meiotic chromosomes. Exp Cell Res *316*, 158-171. 10.1016/j.yexcr.2009.08.007.

Fukuda, T., Fukuda, N., Agostinho, A., Hernandez-Hernandez, A., Kouznetsova, A., and Hoog, C. (2014). STAG3-mediated stabilization of REC8 cohesin complexes promotes chromosome synapsis during meiosis. The EMBO journal *33*, 1243-1255. 10.1002/embj.201387329.

Funaya, C., Samarasinghe, S., Pruggnaller, S., Ohta, M., Connolly, Y., Müller, J., Murakami, H., Grallert, A., Yamamoto, M., Smith, D., et al. (2012). Transient structure associated with the spindle pole body directs meiotic microtubule reorganization in S. pombe. Curr Biol *22*, 562-574. 10.1016/j.cub.2012.02.042.

Ganji, M., Shaltiel, I.A., Bisht, S., Kim, E., Kalichava, A., Haering, C.H., and Dekker, C. (2018). Real-time imaging of DNA loop extrusion by condensin. Science *360*, 102-105. 10.1126/science.aar7831.

Goloborodko, A., Imakaev, M.V., Marko, J.F., and Mirny, L. (2016). Compaction and segregation of sister chromatids via active loop extrusion. Elife *5*. 10.7554/eLife.14864.

Golubovskaya, I.N., Hamant, O., Timofejeva, L., Wang, C.J., Braun, D., Meeley, R., and Cande, W.Z. (2006). Alleles of afd1 dissect REC8 functions during meiotic prophase I. Journal of cell science *119*, 3306-3315. 10.1242/jcs.03054.

Goto, Y., Yamagishi, Y., Shintomi-Kawamura, M., Abe, M., Tanno, Y., and Watanabe, Y. (2017). Pds5 Regulates Sister-Chromatid Cohesion and Chromosome Bi-orientation through a Conserved Protein Interaction Module. Curr Biol *27*, 1005-1012. 10.1016/j.cub.2017.02.066.

Grey, C., and de Massy, B. (2021). Chromosome Organization in Early Meiotic Prophase. Front Cell Dev Biol *9*, 688878. 10.3389/fcell.2021.688878.

Haarhuis, J.H.I., van der Weide, R.H., Blomen, V.A., Yáñez-Cuna, J.O., Amendola, M., van Ruiten, M.S., Krijger, P.H.L., Teunissen, H., Medema, R.H., van Steensel, B., et al. (2017). The Cohesin Release Factor WAPL Restricts Chromatin Loop Extension. Cell *169*, 693-707.e614. 10.1016/j.cell.2017.04.013.

Hiraoka, Y. (2020). Phase separation drives pairing of homologous chromosomes. Curr Genet *66*, 881-887. 10.1007/s00294-020-01077-9.

Hong, S., Joo, J.H., Yun, H., Kleckner, N., and Kim, K.P. (2019). Recruitment of Rec8, Pds5 and Rad61/Wapl to meiotic homolog pairing, recombination, axis formation and S-phase. Nucleic Acids Res *47*, 11691-11708. 10.1093/nar/gkz903.

Hopkins, J., Hwang, G., Jacob, J., Sapp, N., Bedigian, R., Oka, K., Overbeek, P., Murray, S., and Jordan, P.W. (2014). Meiosis-specific cohesin component, Stag3 is essential for maintaining centromere chromatid cohesion, and required for DNA repair and synapsis between homologous chromosomes. PLoS genetics *10*, e1004413. 10.1371/journal.pgen.1004413.

Hore, T.A., Deakin, J.E., and Marshall Graves, J.A. (2008). The evolution of epigenetic regulators CTCF and BORIS/CTCFL in amniotes. PLoS Genet *4*, e1000169. 10.1371/journal.pgen.1000169.

Horie, S., Watanabe, Y., Tanaka, K., Nishiwaki, S., Fujioka, H., Abe, H., Yamamoto, M., and Shimoda, C. (1998). The Schizosaccharomyces pombe mei4+ gene encodes a meiosis-specific transcription factor containing a forkhead DNA-binding domain. Mol Cell Biol *18*, 2118-2129. 10.1128/MCB.18.4.2118.

Hunter, N. (2015). Meiotic Recombination: The Essence of Heredity. Cold Spring Harb Perspect Biol *7*. 10.1101/cshperspect.a016618.

Imakaev, M., Fudenberg, G., McCord, R.P., Naumova, N., Goloborodko, A., Lajoie, B.R., Dekker, J., and Mirny, L.A. (2012). Iterative correction of Hi-C data reveals hallmarks of chromosome organization. Nat Methods *9*, 999-1003. 10.1038/nmeth.2148.

Ishiguro, K., Kim, J., Shibuya, H., Hernandez-Hernandez, A., Suzuki, A., Fukagawa, T., Shioi, G., Kiyonari, H., Li, X.C., Schimenti, J., et al. (2014). Meiosis-specific cohesin mediates homolog recognition in mouse spermatocytes. Genes Dev *28*, 594-607. gad.237313.113 [pii]10.1101/gad.237313.113.

Ishiguro, K.I. (2019). The cohesin complex in mammalian meiosis. Genes Cells *24*, 6-30. 10.1111/gtc.12652.

Ito, M., Kugou, K., Fawcett, J.A., Mura, S., Ikeda, S., Innan, H., and Ohta, K. (2014). Meiotic recombination cold spots in chromosomal cohesion sites. Genes Cells *19*, 359-373. 10.1111/gtc.12138.

Kawashima, S.A., Takemoto, A., Nurse, P., and Kapoor, T.M. (2012). Analyzing fission yeast multidrug resistance mechanisms to develop a genetically tractable model system for chemical biology. Chem Biol *19*, 893-901. 10.1016/j.chembiol.2012.06.008.

Keeney, S. (2001). Mechanism and control of meiotic recombination initiation. Curr Top Dev Biol *52*, 1-53. 10.1016/s0070-2153(01)52008-6.

Kikuchi, S., Borek, D.M., Otwinowski, Z., Tomchick, D.R., and Yu, H. (2016). Crystal structure of the cohesin loader Scc2 and insight into cohesinopathy. Proc Natl Acad Sci U S A *113*, 12444-12449. 10.1073/pnas.1611333113.

Kim, E., Kerssemakers, J., Shaltiel, I.A., Haering, C.H., and Dekker, C. (2020). DNA-loop extruding condensin complexes can traverse one another. Nature *579*, 438-442. 10.1038/s41586-020-2067-5.

Kim, K.D., Tanizawa, H., Iwasaki, O., and Noma, K. (2016). Transcription factors mediate condensin recruitment and global chromosomal organization in fission yeast. Nat Genet *48*, 1242-1252. 10.1038/ng.3647.

Kim, Y., Shi, Z., Zhang, H., Finkelstein, I.J., and Yu, H. (2019). Human cohesin compacts DNA by loop extrusion. Science *366*, 1345-1349. 10.1126/science.aaz4475.

Kitajima, T.S., Yokobayashi, S., Yamamoto, M., and Watanabe, Y. (2003). Distinct cohesin complexes organize meiotic chromosome domains. Science *300*, 1152-1155.

Kleckner, N. (2006). Chiasma formation: chromatin/axis interplay and the role(s) of the synaptonemal complex. Chromosoma *115*, 175-194. 10.1007/s00412-006-0055-7.

Klein, F., Mahr, P., Galova, M., Buonomo, S.B.C., Michaelis, C., Nairz, K., and Nasmyth, K. (1999). A central role for cohesins in sister chromatid cohesion, formation of axial elements, and recombination during yeast meiosis. Cell *98*, 91-103.

Kschonsak, M., Merkel, F., Bisht, S., Metz, J., Rybin, V., Hassler, M., and Haering, C.H. (2017). Structural Basis for a Safety-Belt Mechanism That Anchors Condensin to Chromosomes. Cell *171*, 588-600.e524. 10.1016/j.cell.2017.09.008.

Li, Y., Haarhuis, J.H.I., Sedeño Cacciatore, Á., Oldenkamp, R., van Ruiten, M.S., Willems, L., Teunissen, H., Muir, K.W., de Wit, E., Rowland, B.D., and Panne, D. (2020). The structural basis for cohesin-CTCF-anchored loops. Nature *578*, 472-476. 10.1038/s41586-019-1910-z.

Lieberman-Aiden, E., van Berkum, N.L., Williams, L., Imakaev, M., Ragoczy, T., Telling, A., Amit, I., Lajoie, B.R., Sabo, P.J., Dorschner, M.O., et al. (2009). Comprehensive mapping of long-range interactions reveals folding principles of the human genome. Science *326*, 289-293. 10.1126/science.1181369.

Lin, S.J., and O'Connell, M.J. (2017). DNA Topoisomerase II modulates acetyl-regulation of cohesin-mediated chromosome dynamics. Curr Genet *63*, 923-930. 10.1007/s00294-017-0691-x.

Llano, E., Gomez, H.L., Garcia-Tunon, I., Sanchez-Martin, M., Caburet, S., Barbero, J.L., Schimenti, J.C., Veitia, R.A., and Pendas, A.M. (2014). STAG3 is a strong candidate gene for male infertility. Human molecular genetics *23*, 3421-3431. 10.1093/hmg/ddu051.

Loidl, J. (2006). S. pombe linear elements: the modest cousins of synaptonemal complexes. Chromosoma *115*, 260-271. 10.1007/s00412-006-0047-7.

Lorenz, A., Estreicher, A., Kohli, J., and Loidl, J. (2006). Meiotic recombination proteins localize to linear elements in Schizosaccharomyces pombe. Chromosoma *115*, 330-340. 10.1007/s00412-006-0053-9.

Lorenz, A., Wells, J.L., Pryce, D.W., Novatchkova, M., Eisenhaber, F., McFarlane, R.J., and Loidl, J. (2004). S. pombe meiotic linear elements contain proteins related to synaptonemal complex components. J Cell Sci *117*, 3343-3351. 10.1242/jcs.01203.

Luo, Z., Wang, X., Jiang, H., Wang, R., Chen, J., Chen, Y., Xu, Q., Cao, J., Gong, X., Wu, J., et al. (2020). Reorganized 3D Genome Structures Support Transcriptional Regulation in Mouse Spermatogenesis. iScience *23*, 101034. 10.1016/j.isci.2020.101034.

Mehta, G.D., Kumar, R., Srivastava, S., and Ghosh, S.K. (2013). Cohesin: functions beyond sister chromatid cohesion. FEBS Lett *587*, 2299-2312. 10.1016/j.febslet.2013.06.035.

Miyoshi, T., Ito, M., Kugou, K., Yamada, S., Furuichi, M., Oda, A., Yamada, T., Hirota, K., Masai, H., and Ohta, K. (2012). A central coupler for recombination initiation linking chromosome architecture to S phase checkpoint. Mol Cell *47*, 722-733. 10.1016/j.molcel.2012.06.023.

Mizuguchi, T., Fudenberg, G., Mehta, S., Belton, J.M., Taneja, N., Folco, H.D., FitzGerald, P., Dekker, J., Mirny, L., Barrowman, J., and Grewal, S.I.S. (2014). Cohesin-dependent globules and heterochromatin shape 3D genome architecture in S. pombe. Nature *516*, 432-435. 10.1038/nature13833.

Moore, D.P., and Orr-Weaver, T.L. (1998). Chromosome segregation during meiosis: building an unambivalent bivalent. Curr Top Dev Biol *37*, 263-299.

Moreno, S., Klar, A., and Nurse, P. (1991). Molecular genetic analysis of fission yeast *Schizosaccharomyces pombe*. Methods Enzymol. *194*, 795-823.

Muller, H., Scolari, V.F., Agier, N., Piazza, A., Thierry, A., Mercy, G., Descorps-Declere, S., Lazar-Stefanita, L., Espeli, O., Llorente, B., et al. (2018). Characterizing meiotic chromosomes' structure and pairing using a designer sequence optimized for Hi-C. Mol Syst Biol *14*, e8293. 10.15252/msb.20188293.

Murakami-Tonami, Y., Yamada-Namikawa, C., Tochigi, A., Hasegawa, N., Kojima, H., Kunimatsu, M., Nakanishi, M., and Murakami, H. (2007). Mei4p coordinates the onset of meiosis I by regulating cdc25+ in fission yeast. Proc Natl Acad Sci U S A *104*, 14688-14693. 10.1073/pnas.0702906104.

Nagaoka, S.I., Hassold, T.J., and Hunt, P.A. (2012). Human aneuploidy: mechanisms and new insights into an age-old problem. Nat Rev Genet *13*, 493-504. 10.1038/nrg3245.

Nasmyth, K. (2001). Disseminating the genome: joining, resolving, and separating sister chromatids during mitosis and meiosis. Annu. Rev. Genet. *35*, 673-745.

Nora, E.P., Goloborodko, A., Valton, A.L., Gibcus, J.H., Uebersohn, A., Abdennur, N., Dekker, J., Mirny, L.A., and Bruneau, B.G. (2017). Targeted Degradation of CTCF Decouples Local Insulation of Chromosome Domains from Genomic Compartmentalization. Cell *169*, 930-944.e922. 10.1016/j.cell.2017.05.004.

Olson, L.W., Eden, U., Egel-Mitani, M., and Egel, R. (1978). Asynaptic meiosis in fission yeast? Hereditas *89*, 189-199.

Pasierbek, P., Jantsch, M., Melcher, M., Schleiffer, A., Schweizer, D., and Loidl, J. (2001). A Caenorhabditis elegans cohesion protein with functions in meiotic chromosome pairing and disjunction. Genes & development *15*, 1349-1360.

Patel, L., Kang, R., Rosenberg, S.C., Qiu, Y., Raviram, R., Chee, S., Hu, R., Ren, B., Cole, F., and Corbett, K.D. (2019). Dynamic reorganization of the genome shapes the recombination landscape in meiotic prophase. Nat Struct Mol Biol *26*, 164-174. 10.1038/s41594-019-0187-0.

Pelttari, J., Hoja, M.R., Yuan, L., Liu, J.G., Brundell, E., Moens, P., Santucci-Darmanin, S., Jessberger, R., Barbero, J.L., Heyting, C., and Höög, C. (2001). A meiotic chromosomal core consisting of cohesin complex proteins recruits DNA recombination proteins and promotes synapsis in the absence of an axial element in mammalian meiotic cells. Mol Cell Biol *21*, 5667-5677. 10.1128/MCB.21.16.5667-5677.2001.

Peters, J.M., and Nishiyama, T. (2012). Sister chromatid cohesion. Cold Spring Harb Perspect Biol *4*. 10.1101/cshperspect.a011130.

Petronczki, M., Siomos, M.F., and Nasmyth, K. (2003). Un menage a quatre: the molecular biology of chromosome segregation in meiosis. Cell *112*, 423-440.

Phadnis, N., Cipak, L., Polakova, S., Hyppa, R.W., Cipakova, I., Anrather, D., Karvaiova, L., Mechtler, K., Smith, G.R., and Gregan, J. (2015). Casein Kinase 1 and Phosphorylation of Cohesin Subunit Rec11 (SA3) Promote Meiotic Recombination through Linear Element Formation. PLoS Genet *11*, e1005225. 10.1371/journal.pgen.1005225.

Ponticelli, A.S., and Smith, G.R. (1992). Chromosomal context dependence of a eukaryotic recombinational hot spot. Proc Natl Acad Sci U S A *89*, 227-231. 10.1073/pnas.89.1.227.

Rabitsch, K.P., Toth, A., Galova, M., Schleiffer, A., Schaffner, G., Aigner, E., Rupp, C., Penkner, A.M., Moreno-Borchart, A.C., Primig, M., et al. (2001). A screen for genes required for meiosis and spore formation based on whole-genome expression. Current biology : CB *11*, 1001-1009.

Rao, S.S., Huntley, M.H., Durand, N.C., Stamenova, E.K., Bochkov, I.D., Robinson, J.T., Sanborn, A.L., Machol, I., Omer, A.D., Lander, E.S., and Aiden, E.L. (2014). A 3D map of the human genome at kilobase resolution reveals principles of chromatin looping. Cell *159*, 1665-1680. 10.1016/j.cell.2014.11.021.

Rao, S.S.P., Huang, S.C., Glenn St Hilaire, B., Engreitz, J.M., Perez, E.M., Kieffer-Kwon, K.R., Sanborn, A.L., Johnstone, S.E., Bascom, G.D., Bochkov, I.D., et al. (2017). Cohesin Loss Eliminates All Loop Domains. Cell *171*, 305-320.e324. 10.1016/j.cell.2017.09.026.

Ruan, K., Yamamoto, T.G., Asakawa, H., Chikashige, Y., Masukata, H., Haraguchi, T., and Hiraoka, Y. (2015). Meiotic nuclear movements in fission yeast are regulated by the transcription factor Mei4 downstream of a Cds1-dependent replication checkpoint pathway. Genes Cells *20*, 160-172. 10.1111/gtc.12207.

Sakuno, T., and Watanabe, Y. (2015). Phosphorylation of cohesin Rec11/SA3 by casein kinase 1 promotes homologous recombination by assembling the meiotic chromosome axis. Dev Cell *32*, 220-230. 10.1016/j.devcel.2014.11.033.

Sanborn, A.L., Rao, S.S., Huang, S.C., Durand, N.C., Huntley, M.H., Jewett, A.I., Bochkov, I.D., Chinnappan, D., Cutkosky, A., Li, J., et al. (2015). Chromatin extrusion explains key features of loop and domain formation in wild-type and engineered genomes. Proc Natl Acad Sci U S A *112*, E6456-6465. 10.1073/pnas.1518552112.

Sato, M., Dhut, S., and Toda, T. (2005). New drug-registant cassettes for gene disruption and epitope tagging in Schizosaccharomyces pombe. Yeast *22*, 583-591.

Schalbetter, S.A., Fudenberg, G., Baxter, J., Pollard, K.S., and Neale, M.J. (2019). Principles of meiotic chromosome assembly revealed in S. cerevisiae. Nat Commun *10*,

4795. 10.1038/s41467-019-12629-0.

Schindelin, J., Arganda-Carreras, I., Frise, E., Kaynig, V., Longair, M., Pietzsch, T., Preibisch, S., Rueden, C., Saalfeld, S., Schmid, B., et al. (2012). Fiji: an open-source platform for biological-image analysis. Nat Methods *9*, 676-682. 10.1038/nmeth.2019.

Sharif, W.D., Glick, G.G., Davidson, M.K., and Wahls, W.P. (2002). Distinct functions of S. pombe Rec12 (Spo11) protein and Rec12-dependent crossover recombination (chiasmata) in meiosis I; and a requirement for Rec12 in meiosis II. Cell Chromosome *1*, 1. 10.1186/1475-9268-1-1.

Silva, M.C.C., Powell, S., Ladstätter, S., Gassler, J., Stocsits, R., Tedeschi, A., Peters, J.M., and Tachibana, K. (2020). Wapl releases Scc1-cohesin and regulates chromosome structure and segregation in mouse oocytes. J Cell Biol *219*. 10.1083/jcb.201906100.

Takao, K., Takamiya, K., Ding, D., Haraguchi , T., Hiraoka, Y., Nishimori, H., and Awazu, A. (2019). Torsional Turning Motion of Chromosomes as an Accelerating Force to Align Homologous Chromosomes during Meiosis. Journal of the Physical Society of Japan *88* (*023801*).

Tanizawa, H., Kim, K.D., Iwasaki, O., and Noma, K.I. (2017). Architectural alterations of the fission yeast genome during the cell cycle. Nat Struct Mol Biol *24*, 965-976. 10.1038/nsmb.3482.

Tedeschi, A., Wutz, G., Huet, S., Jaritz, M., Wuensche, A., Schirghuber, E., Davidson, I.F., Tang, W., Cisneros, D.A., Bhaskara, V., et al. (2013). Wapl is an essential regulator of chromatin structure and chromosome segregation. Nature *501*, 564-568. 10.1038/nature12471.

Terakawa, T., Bisht, S., Eeftens, J.M., Dekker, C., Haering, C.H., and Greene, E.C. (2017). The condensin complex is a mechanochemical motor that translocates along DNA. Science *358*, 672-676. 10.1126/science.aan6516.

Viera, A., Berenguer, I., Ruiz-Torres, M., Gómez, R., Guajardo, A., Barbero, J.L., Losada, A., and Suja, J.A. (2020). PDS5 proteins regulate the length of axial elements and telomere integrity during male mouse meiosis. EMBO Rep *21*, e49273. 10.15252/embr.201949273.

Wang, Y., Wang, H., Zhang, Y., Du, Z., Si, W., Fan, S., Qin, D., Wang, M., Duan, Y., Li, L., et al. (2019). Reprogramming of Meiotic Chromatin Architecture during Spermatogenesis. Mol Cell *73*, 547-561.e546. 10.1016/j.molcel.2018.11.019.

Webster, A., and Schuh, M. (2017). Mechanisms of Aneuploidy in Human Eggs. Trends Cell Biol *27*, 55-68. 10.1016/j.tcb.2016.09.002.

Winters, T., McNicoll, F., and Jessberger, R. (2014). Meiotic cohesin STAG3 is required for chromosome axis formation and sister chromatid cohesion. The EMBO journal *33*,

1256-1270. 10.1002/embj.201387330.

Wutz, G., Várnai, C., Nagasaka, K., Cisneros, D.A., Stocsits, R.R., Tang, W., Schoenfelder, S., Jessberger, G., Muhar, M., Hossain, M.J., et al. (2017). Topologically associating domains and chromatin loops depend on cohesin and are regulated by CTCF, WAPL, and PDS5 proteins. EMBO J *36*, 3573-3599. 10.15252/embj.201798004.

Xu, H., Beasley, M.D., Warren, W.D., van der Horst, G.T., and McKay, M.J. (2005). Absence of mouse REC8 cohesin promotes synapsis of sister chromatids in meiosis. Developmental cell *8*, 949-961.

Yamamoto, A., and Hiraoka, Y. (2001). How do meiotic chromosomes meet their homologous partners?: lessons from fission yeast. Bioessays *23*, 526-533. 10.1002/bies.1072.

Yamamoto, A., and Hiraoka, Y. (2003). Monopolar spindle attachment of sister chromatids is ensured by two distinct mechanisms at the first meiotic division in fission yeast. EMBO J *22*, 2284-2296. 10.1093/emboj/cdg222.

Yokobayashi, S., and Watanabe, Y. (2005). The kinetochore protein Moa1 enables cohesion-mediated monopolar attachment at meiosis I. Cell *123*, 803-817.

Yokobayashi, S., Yamamoto, M., and Watanabe, Y. (2003). Cohesins determine the attachment manner of kinetochores to spindle microtubules at meiosis I in fission yeast. Mol Cell Biol *23*, 3965-3973. 10.1128/MCB.23.11.3965-3973.2003.

Young, J.A., Hyppa, R.W., and Smith, G.R. (2004). Conserved and nonconserved proteins for meiotic DNA breakage and repair in yeasts. Genetics *167*, 593-605. 10.1534/genetics.103.023762.

Zickler, D., and Kleckner, N. (1999). Meiotic chromosomes: integrating structure and function. Annu Rev Genet *33*, 603-754. 10.1146/annurev.genet.33.1.603.

Figure 1. Hi-C analysis firmly recapitulates the structure of meiotic bouquet chromosomes.

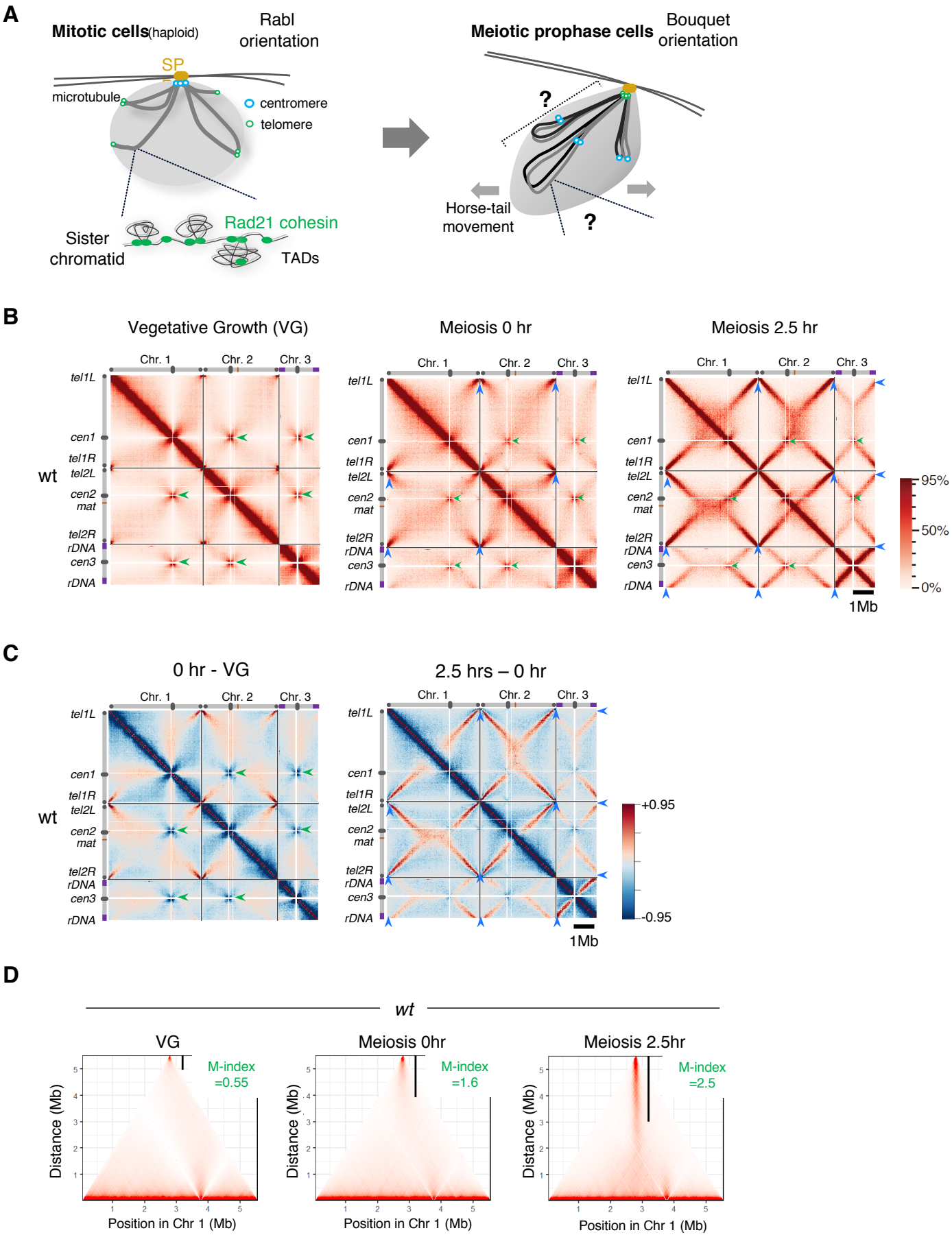

Figure 2. Rec8 cohesin shapes chromosomes into a structure suitable for its alignment

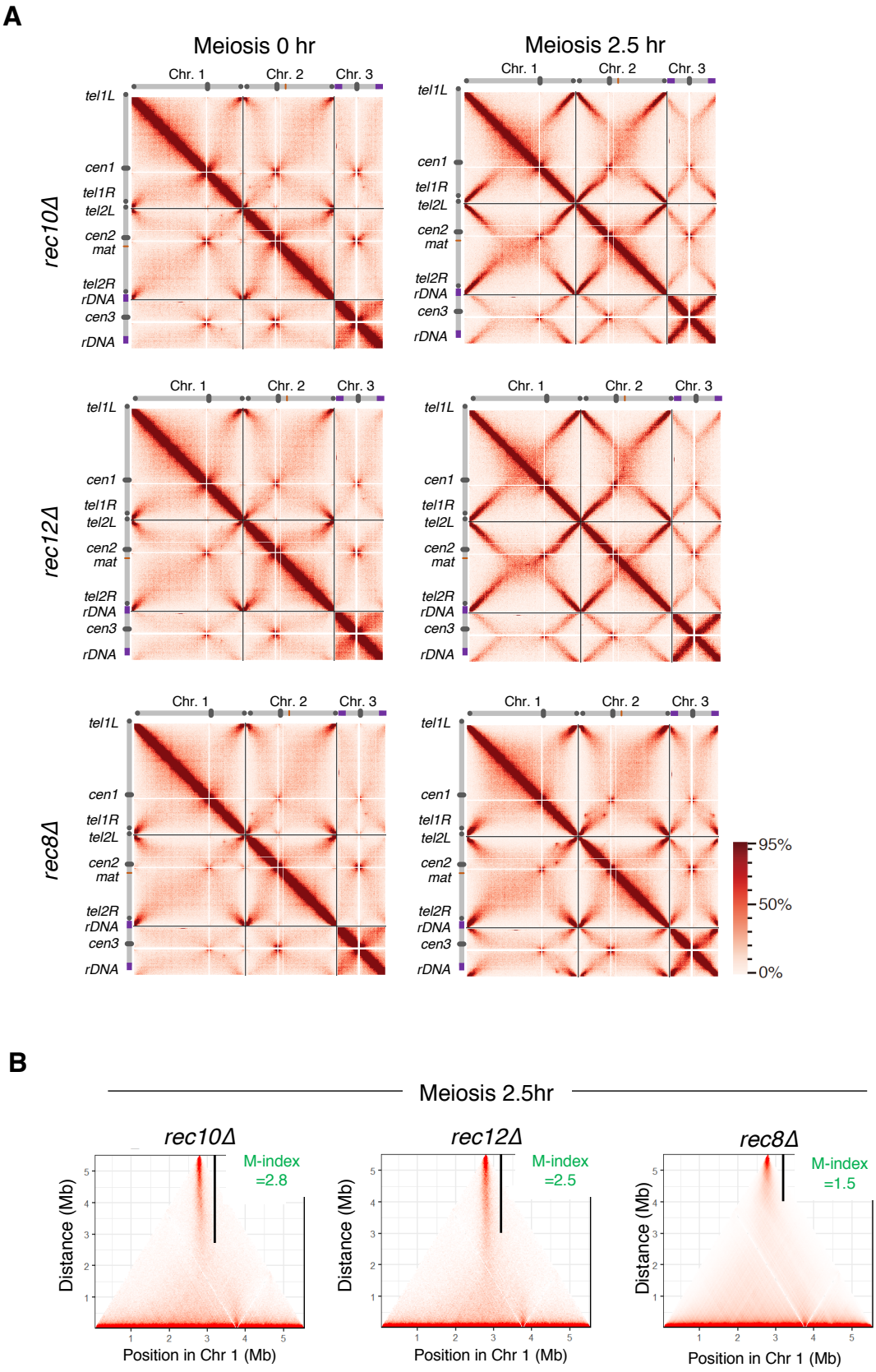

Figure 3. Rec8 cohesin is crucial to construct the meiosis-specific chromatin loops.

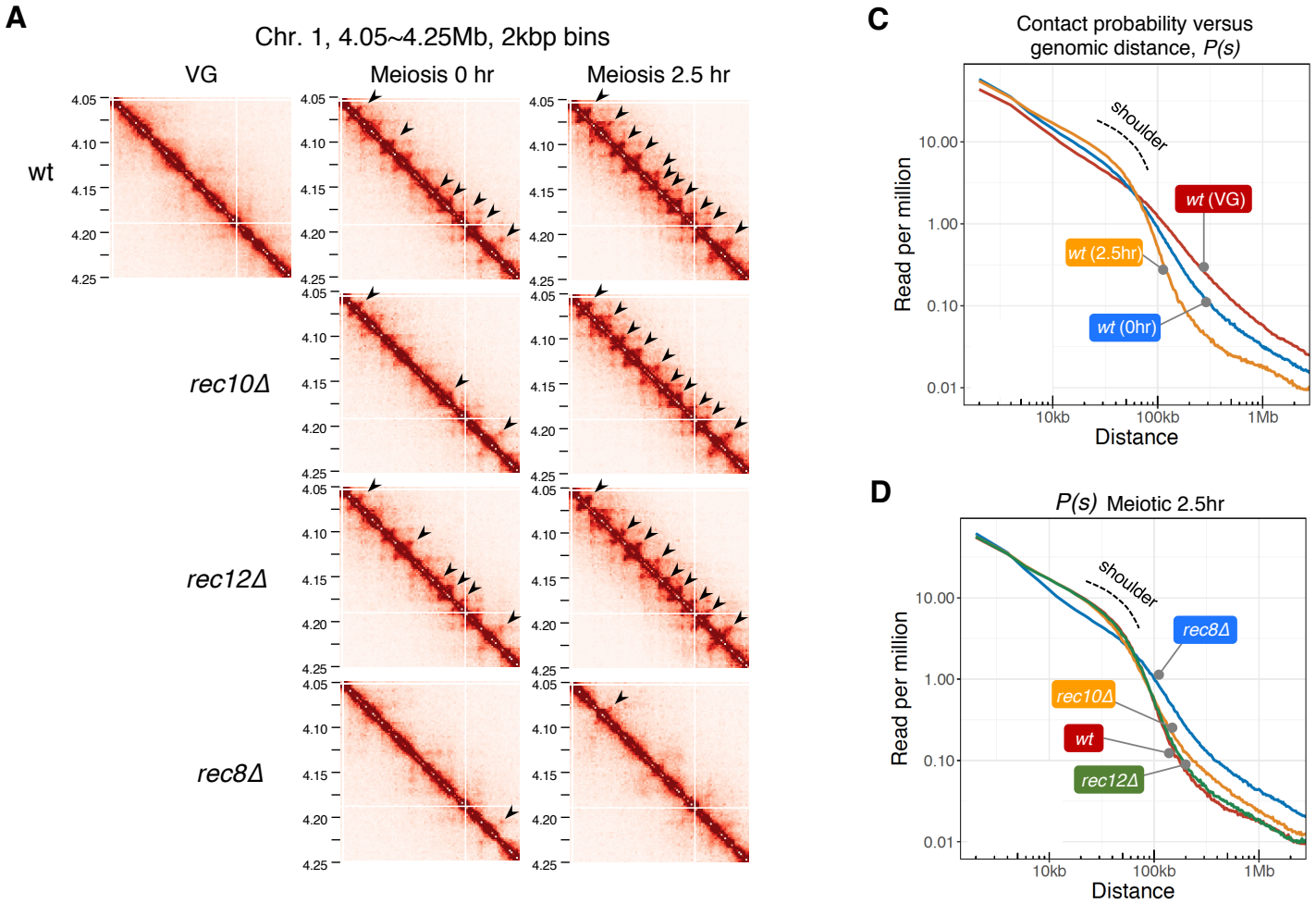

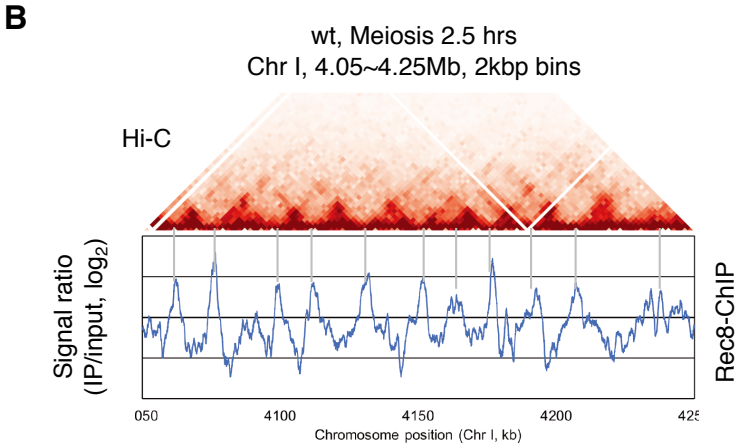

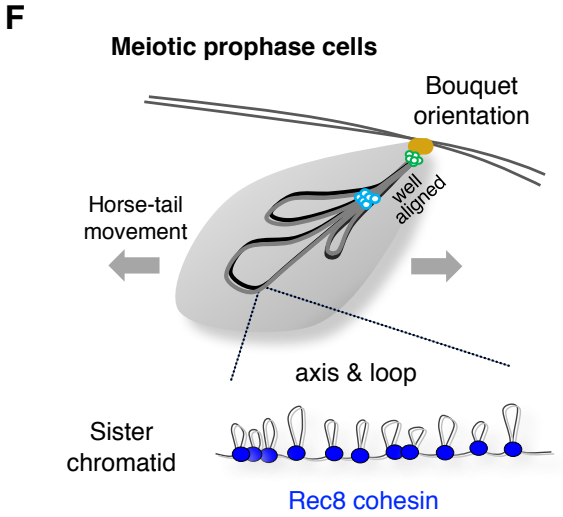

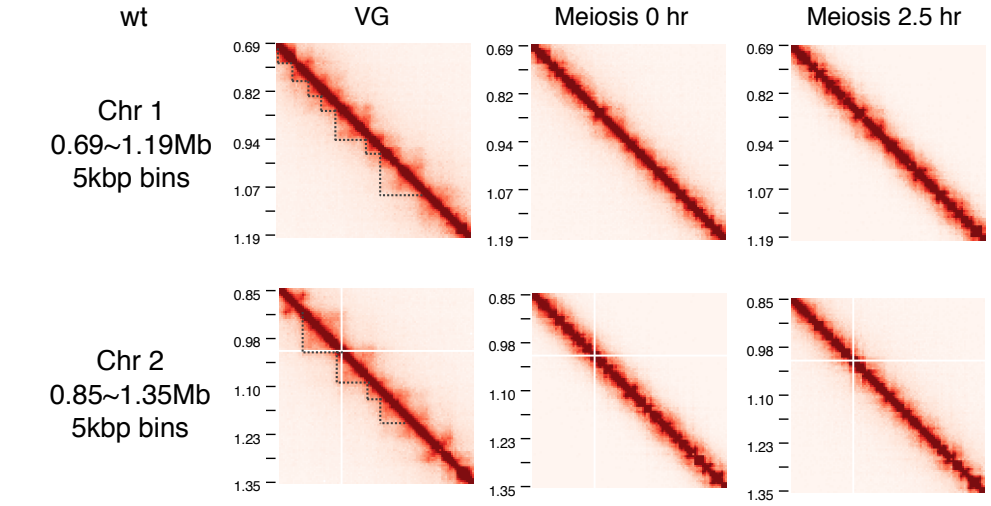

Figure 4. Wpl1 regulates chromatin loop length during meiotic prophase in *S. pombe*.

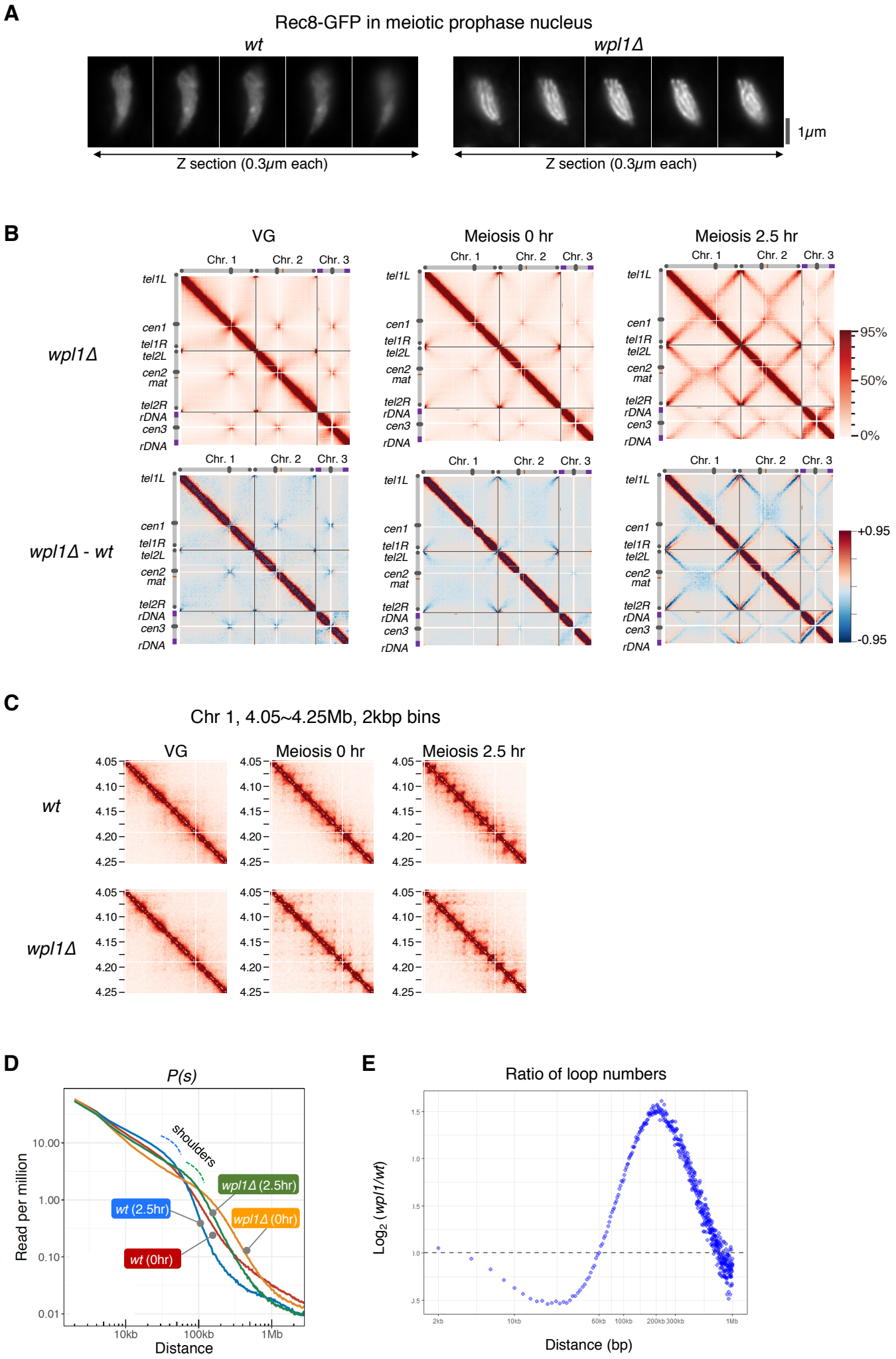

Figure 5. Isolation of *rec8* mutant showing defect in axis formation with intact cohesion function

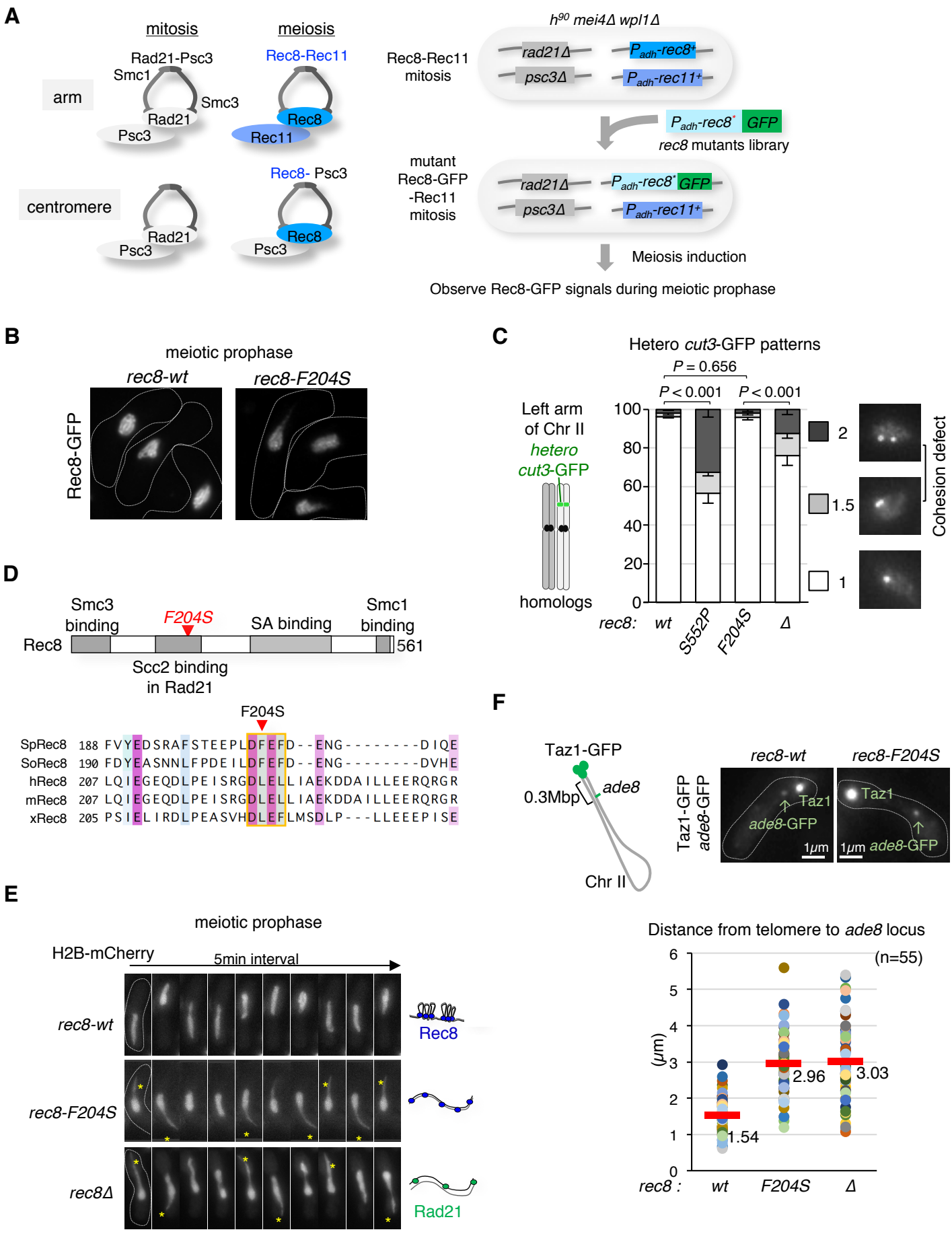

Figure 6. *rec8-F204S* mutant displays defective chromatin loop formation

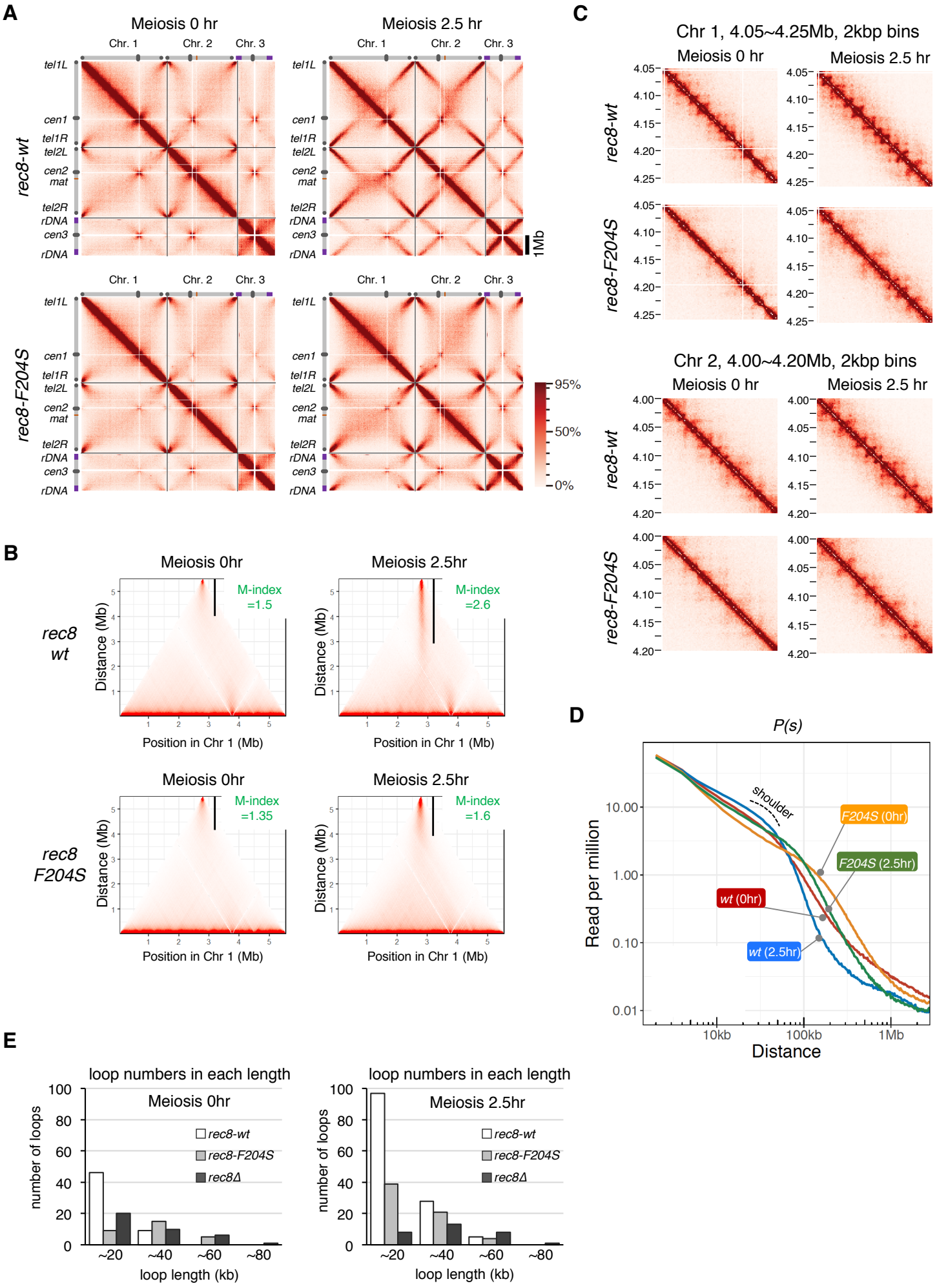
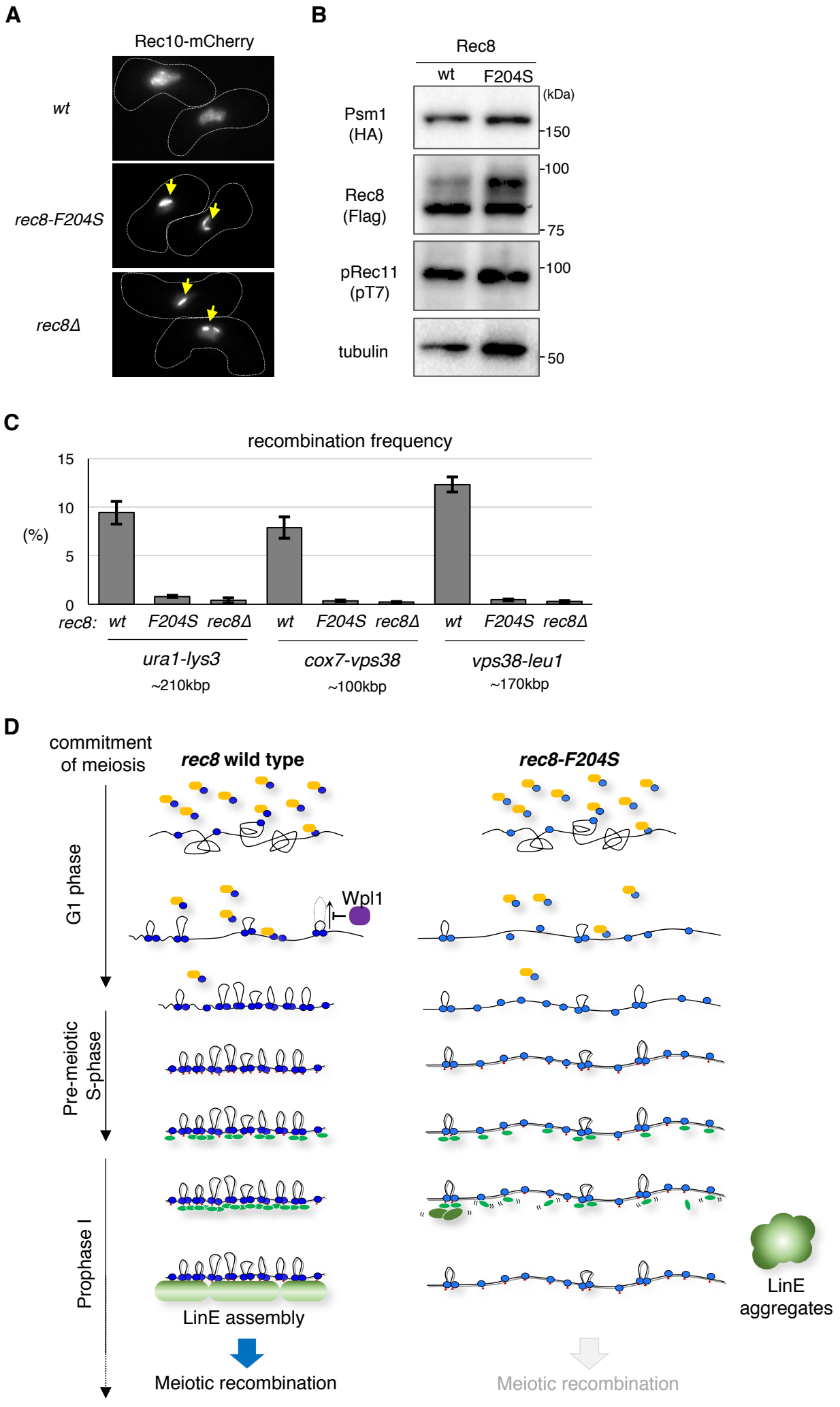
Figure 7. Rec8-dependent chromatin loop formation and meiotic recombination